



TAMPERE UNIVERSITY OF TECHNOLOGY

KIRSI HUTTUNEN
EXCITED-STATE INTRAMOLECULAR PROTON TRANSFER
IN 10-HYDROXYBENZO[*h*]QUINOLINE DERIVATIVES

Master of Science Thesis

Examiner: Prof. Nikolai V. Tkachenko
Examiner and topic approved by
the Faculty Council of the Faculty of
Science and Environmental Engineering
on 9 November 2011

ABSTRACT

TAMPERE UNIVERSITY OF TECHNOLOGY

Master's Degree Programme in Science and Engineering

HUTTUNEN, KIRSI: Excited-State Intramolecular Proton Transfer in 10-Hydroxybenzo[*h*]quinoline Derivatives

Master of Science Thesis, 57 pages, 10 Appendix pages

February 2012

Major: Chemistry

Examiner: Professor Nikolai V. Tkachenko

Keywords: excited-state intramolecular proton transfer, 10-hydroxybenzo[*h*]quinoline, time-resolved fluorescence spectroscopy

If a molecule contains a proton donor and a proton acceptor group in close proximity, an intramolecular hydrogen bond may be formed between the groups. Upon electronic excitation, a proton transfer from the donor to the acceptor is possible. This process is called an excited-state intramolecular proton transfer (ESIPT).

The ESIPT processes can be studied with spectroscopic techniques, because the different tautomers of an ESIPT compound have different spectroscopic properties. The energy difference between the ground state and first excited state is smaller for the proton transfer tautomer than for the normal tautomer, and thus the fluorescence bands of these two species are located at quite different wavelengths.

One of the most promising compounds for ESIPT applications is 10-hydroxybenzo[*h*]quinoline (HBQ). Due to its restricted geometry and the specific alignment of oxygen and nitrogen atoms, this compound possesses an exceptionally strong intramolecular hydrogen bond. Thus, the ESIPT reaction is fast and does not suffer from solvent perturbation, not even in protic solvents.

In this Thesis, a systematic study on the substituent effect on the ESIPT kinetics of HBQ derivatives is presented. The used measurement techniques include steady-state absorption and emission spectroscopy as well as time-resolved methods for determining fluorescence lifetimes. Several different HBQ derivatives are studied, and the performance of compounds with different substituents at the same position is compared. Furthermore, the effect of solvent polarity on the ESIPT rate is investigated by repeating the measurements in solvents with different polarities.

ESIPT is reported to occur in most of the studied compounds. An electron-donating substituent at the methylenepyridine part of the molecule shifts the fluorescence emission of the proton transfer tautomer to shorter wavelengths compared to the non-substituted HBQ. An electron-withdrawing substituent has the opposite effect, respectively. Furthermore, the electron-withdrawing substituents induce an increase in the relaxation rate of the proton transfer tautomer, caused by the lowered basicity and proton-binding ability of the proton acceptor moiety.

A remarkable solvent effect in the proton transfer relaxation rate is observed only for two compounds with a nitro substituent. Perhaps the position and the electron-withdrawing character of the substituent weaken the intramolecular hydrogen bond in these compounds, making it more vulnerable to perturbation by polar solvents.

TIIVISTELMÄ

TAMPEREEN TEKNILLINEN YLIOPISTO

Teknis-luonnontieteellinen koulutusohjelma

**HUTTUNEN, KIRSI: Molekyylin sisäinen virittyneen tilan protoninsiirto
10-hydroksibentso[h]kinoliinijohdannaisissa**

Diplomityö, 57 sivua, 10 liitesivua

Helmikuu 2012

Pääaine: Kemia

Tarkastaja: professori Nikolai V. Tkachenko

Avainsanat: virittyneen tilan protoninsiirto, 10-hydroksibentso[h]kinoliini, aikaerotteinen fluoresenssispektroskopia

Jos molekyyli sisältää protonidonorin ja protoniakseptorin lähekkäin toisiaan, näiden ryhmien välille voi syntyä molekyylin sisäinen vetysidos. Kun molekyyli viritetään elektronisesti, protoni voi siirtyä donorilta akseptorille. Tätä prosessia kutsutaan molekyylin sisäiseksi virittyneen tilan protoninsiirroksi.

Protoninsiirtoreaktioita voidaan tutkia spektroskopisin menetelmin, sillä molekyylien eri tautomeerit käyttäytyvät spektroskopisesti hyvin eri tavoin. Perustilan ja virittyneen tilan välinen energiaero on pienempi tautomeerilla, jossa protoni on siirtynyt, kuin molekyylin normaalimuodolla. Siten eri tautomeerien fluoresenssi havaitaan eri aallonpituuksilla.

Yksi lupaavimmista yhdisteistä protoninsiirtoa hyödyntäviin sovelluksiin on 10-hydroksibentso[h]kinoliini (HBQ, engl. 10-hydroxybenzo[h]quinoline). Molekyylin geometria pakottaa protonidonorin ja -akseptorin hyvin lähelle toisiaan, joten tässä yhdisteessä molekyylin sisäinen vetysidos on poikkeuksellisen vahva. Protoninsiirtoreaktio on siten hyvin nopea, ja se tapahtuu jopa proottisissa liuottimissa.

Tässä diplomityössä tutkitaan systemaattisesti substituenttien vaikutusta protoninsiirtoreaktion kinetiikkaan HBQ-johdannaisissa. Tutkimusmenetelminä käytetään absorptio- ja emissiospektroskopiaa sekä aikaerotteista fluoresenssispektroskopiaa. Tutkittavana on useita HBQ-johdannaisia, ja samassa kohdassa molekyyliä sijaitsevien erilaisten substituenttien vaikutusta protoninsiirtoon vertaillaan. Lisäksi liuottimen poolisuuden vaikutusta protoninsiirtoreaktion nopeuteen tutkitaan toistamalla mittaukset useassa liuottimessa.

Protoninsiirtoreaktio havaitaan lähes kaikissa tutkituissa yhdisteissä. Elektroneja luovuttava ryhmä molekyylin metyleenipyridiiniolosassa aiheuttaa emission siirtymisen lyhyemmille aallonpituuksille kuin substituomattomassa yhdisteessä. Vastaavasti, elektroneja puoleensa vetävällä ryhmällä on vastakkainen vaikutus. Lisäksi, elektroneja puoleensa vetävät substituentit nopeuttavat protoninsiirtotautomeerin relaksaatiota. Tämä johtuu protoniakseptorin heikommasta emäksisyydestä, mikä vaikeuttaa protonin sitoutumista siihen.

Liuottimen poolisuuden havaitaan vaikuttavan protoninsiirtoon vain yhdisteissä, joissa on nitroryhmä. Ryhmän paikka ja elektroneja puoleensa vetävä luonne heikentävät molekyylin sisäistä vetysidosta, jolloin pooliset liuottimet häiritsevät protoninsiirtoa.

PREFACE

This Master of Science Thesis was done at the Department of Chemistry and Bioengineering, at Tampere University of Technology, from May to December 2011.

First, I would like to thank the Head of the Supramolecular Photochemistry Laboratory, Professor Helge Lemmetyinen for the opportunity to work at the Laboratory, first as a summer student and then continue to the Master's Thesis. I would also like to express my gratitude to Professor Nikolai V. Tkachenko for supervising my work, and for the guidance into the world of ultrafast spectroscopy. The research group of Dr. Daniel Gryko at the Institute of Organic Chemistry at Polish Academy of Sciences receive my compliment for the HBQ derivatives.

I would also like to thank the my co-workers at the Spectroscopy team. A special thanks goes to Riitta for the supporting conversations at the office. With you as a colleague, even the most difficult days turned brighter. To all my friends, I want to express my gratitude for the memorable and hilarious moments during the years.

Finally, I would like to thank my loving fiancé, Matti, for your support and patience. During the years, you have surprised me over and over again with the passion you have in everything you do. Don't let that passion ever die.

Lopuksi haluan kiittää vanhempiani. Olette aina olleet tukenani, vaikka opiskelut veivätkin minut kauas kotoa.

Tampere, 10th January, 2012

Kirsi Huttunen

CONTENTS

1	Introduction	1
2	Theoretical background	3
2.1	Absorption of a photon	3
2.1.1	Electronic transitions in a molecule	3
2.1.2	Absorption in a bulk medium	6
2.2	Relaxation of the excited state	8
2.2.1	Relaxation mechanisms of the excited state	8
2.2.2	Quantum yields and lifetimes	11
2.3	Excited-state intramolecular proton transfer	13
2.3.1	Proton transfer compounds	14
2.3.2	Proton transfer reaction	15
2.3.3	Reaction mechanism	16
2.3.4	Substituent effects	18
2.3.5	Solvent effects	19
2.3.6	Possible applications	21
3	Research methods and materials	23
3.1	Measurement methods	23
3.1.1	Steady-state spectroscopy	23
3.1.2	Time-resolved spectroscopy	28
3.2	Materials	32
3.3	Experimental	33
3.3.1	Absorption and emission spectra	34
3.3.2	Fluorescence quantum yields	36
3.3.3	Time-resolved measurements	38
4	Results and discussion	39
4.1	Steady-state measurements	39
4.1.1	Fluorescence quantum yields	40
4.1.2	Substituent effects	42
4.1.3	Solvent effects	43
4.2	Time-resolved measurements	45
4.2.1	4-morpholino-HBQ, 4-methyl-HBQ, and 7-nitro-HBQ	46
4.2.2	4-cyano-HBQ, 4-tosyl-HBQ, and DHB[<i>a,c</i>]P	50
5	Conclusions	52
	Bibliography	54
	Appendices	58

ABBREVIATIONS AND NOTATION

α	Absorption coefficient
ε	Molar absorption coefficient
λ	Wavelength
λ_{em}	Fluorescence emission monitoring wavelength
λ_{ex}	Excitation wavelength
ν	Frequency
$\bar{\nu}$	Wave number
τ_i	Lifetime for a process i
Φ_i	Quantum yield for a process i
3HF	4'- <i>N,N</i> -diethylamino-3-hydroxyflavone
A, A	Absorbance, Acceptor
c	Speed of light, Concentration
CFD	Constant Fraction Discriminator
D	Donor, Detector
DCM	Dichloromethane
DHBP	1,8-Dihydroxybenzophenazine
diCN-HBO	2-{[2-(2-Hydroxyphenyl)benzo[<i>d</i>]oxazol-6-yl]methylene}malononitrile
DNA	Deoxyribonucleic acid
E	Energy
e	Napier's constant
E_f	Energy of a final state after transition
E_i	Energy of an initial state before transition
ESDPT	Excited-State Double Proton Transfer
ESIPT	Excited-State Intramolecular Proton Transfer
FCU	Fiber Coupling Unit
GFP	Green Fluorescent Protein
h	Planck constant
HBA	Hydroxybenzo[<i>c</i>]acridine
HBQ	10-Hydroxybenzo[<i>h</i>]quinoline
HOMO	Highest Occupied Molecular Orbital
HPLC	High-Pressure Liquid Chromatography
I	Intensity
I_F	Fluorescence intensity
I_{in}	Intensity of light entering an absorbing medium
I_{out}	Intensity of light leaving an absorbing medium
IC	Internal conversion
ISC	Intersystem crossing

IUPAC	International Union of Pure and Applied Chemistry
k_i	Rate constant for a process i
k_{nr}	Non-radiative rate constant
k_r	Radiative rate constant
L	Lens
l	Optical path length
LCD	Liquid Crystal Display
LUMO	Lowest Unoccupied Molecular Orbital
M	Mirror
m_s	Spin quantum number of one electron
M_S	Sum of the spin quantum numbers of individual electrons
MeCN	Acetonitrile
MCA	Multichannel Analyzer
MS	Methyl salicylate
NLC	Non-linear crystal
OLED	Organic Light-Emitting Diode
PD	Photodiode
PM	Photomultiplier
PP	5-(2-Pyridyl)-1-H-pyrazole
R	Baseline spectrum of a spectrophotometer
S, S	Total spin quantum number of a molecule, Slit
s	Voltage sensitivity of a photodetector
S_0	Electronic ground state of a molecule
S'_0	Ground state of the proton transfer tautomer
S'_1	First singlet excited state of the proton transfer tautomer
S_c	Spectral correction function
S_n	n^{th} singlet excited state of a molecule
SHG	Second Harmonic Generator
T	Transmittance
T_n	n^{th} triplet state of a molecule
TAC	Time-to-Amplitude Converter
TCSPC	Time-Correlated Single Photon Counting
THF	Tetrahydrofuran
U	Output voltage of a photomultiplier tube
UC	Up-conversion
VR	Vibrational relaxation

1 INTRODUCTION

Transfer of a proton from a donor to an acceptor is one of the most simple chemical reactions one can think of. It is said to be “the most general and important reaction in chemistry” [1, see 2]. Proton transfer processes form the base of acid–base reactions and operation of enzymes, for example [3, pp. 226–275; 4].

In most cases, the proton transfer occurs between two different species. For example in acid dissociation in water, the acid molecule passes the proton to an adjacent water molecule [3, pp. 226–275]. However, if a molecule contains both a proton donor and a proton acceptor group in close proximity to each other, an intramolecular hydrogen bond is formed between the groups [2; 5, p. 238]. Then, it is possible for the proton to move from the donor to the acceptor. The proton transfer is often initiated by electronic excitation of the molecule, for example by a photon [5, p. 238]. Such a photo-initiated, intramolecular process is widely referred to as an *excited-state intramolecular proton transfer* (ESIPT).

The ESIPT processes are easily observed with spectroscopic techniques, because the different tautomers of an ESIPT compound behave quite differently under illumination. Fluorescence of the compounds is observed at wavelengths remarkably longer than the excitation, which corresponds to a smaller energy difference between the ground and excited states in the proton-transfer tautomer [2].

One of the most promising compounds for an ESIPT reaction is 10-hydroxybenzo- $[h]$ quinoline (HBQ). Due to its restricted geometry and the specific alignment of oxygen and nitrogen atoms, the compound possesses an exceptionally strong intramolecular hydrogen bond between a hydroxyl proton and a pyridyl nitrogen. Thus, the ESIPT reaction is fast and does not suffer from solvent perturbation, not even in protic solvents. [5, pp. 242–243] The solvent polarity independent proton transfer process makes HBQ a promising fluorescence label in aqueous solvents and in biochemical environments [6, 7]. Furthermore, the large Stokes shift and low self-absorption enable the use of the compound in radiation-hard scintillator counters [8, see 9] and laser dyes [10, 11], for example.

The effects of solvent polarity and substituents attached to the HBQ core have been studied previously. Chou *et al.* have studied the kinetics of the ESIPT in HBQ both in aqueous solutions and in non-polar hydrocarbon environment [9, 12]. Furthermore, a hypothesis concerning the effect of substitution of the HBQ core on

the HOMO–LUMO energy difference in the compound has been proposed [11]. In the study, the effect of different substituents at the oxygen-containing cyclohexa-2,4-dienone part of the molecule on the spectroscopical properties was investigated. However, the hypothesis has not been experimentally tested for substitution at the nitrogen-containing methylenepyridine part of the molecule.

The solvent and substituent effects on the ESIPT in HBQ have not been previously investigated in a combined study. This Thesis provides a systematic study on the kinetics of the ESIPT process of several HBQ derivatives in solvent environments with different polarities. First, the spectroscopic properties of ten different HBQ derivatives, synthesized by Dr. Daniel T. Gryko and co-workers, are studied in three solvents with different polarities by steady-state methods. For selected compounds with either electron-donating or electron-withdrawing substituents at the methylenepyridine part of the molecule, the effect of the different substitution on the spectroscopic properties is studied by time-resolved methods. In the latter part of the study, solvent effect on the ESIPT kinetics is also investigated by repeating the measurements in different solvents.

2 THEORETICAL BACKGROUND

This Chapter is contentually divided in two parts. First, typical photophysical phenomena such as electronic excitation, absorption, relaxation and fluorescence are discussed. Understanding these processes is vital for being able to discuss photochemical reactions. The second part concentrates on the excited-state intramolecular proton transfer process. Requirements for the ES IPT compounds are introduced, and the reaction mechanism as well as substituent and solvent effects are discussed. Finally, some possible applications for ES IPT compounds are briefly introduced.

2.1 Absorption of a photon

Every photoinduced event starts with the absorption of a photon in a photoactive molecule. In the absorption process, energy of the photon is transferred to the molecule, promoting the molecule to an electronically excited state. The absorption takes place only if the energy of the photon matches the energy difference between the initial and final states, ΔE :

$$\Delta E = E_f - E_i = h\nu = \frac{hc}{\lambda}, \quad (2.1)$$

where E_f and E_i are the energies of the final and initial states, respectively, ν is the frequency of the photon, λ is the corresponding wavelength, h is the Planck constant, and c is the speed of light. [13, p. 955]

Absorption can generate many interesting phenomena in a molecule, giving rise to the fields of photophysics and photochemistry. The consequences of absorption are discussed further in the following sections, together with some quantitative tools for describing and analyzing the process.

2.1.1 Electronic transitions in a molecule

Absorption is essentially a transition between two electronic states in a molecule; from the ground state molecular orbital to an orbital lying higher in energy. In the electronic ground state, the electron with the highest energy occupies the so-called HOMO level (Highest Occupied Molecular Orbital). The transition with the smallest possible energy is always initiated from the HOMO level and ends at the LUMO level (Lowest Unoccupied Molecular Orbital). [14, p. 21]

The concepts of HOMO and LUMO give information only on the ground-state population of two molecular orbitals, but do not describe other properties of the orbitals. The orbitals comprising the HOMO and LUMO levels might have either σ or π character, or might sometimes even be of n type. The σ orbitals are formed either from two s atomic orbitals, or an s orbital and a p orbital, or two p orbitals with collinear symmetry, whereas the π orbitals are formed from two p atomic orbitals with lateral overlap. Each orbital type is split into the bonding and antibonding orbitals, denoted by σ and π for the bonding orbitals, and σ^* and π^* for the antibonding orbitals, respectively. An n orbital is an atomic orbital on an electron-rich atom such as oxygen or nitrogen, having neither bonding nor antibonding character. [14, pp. 20–23]

Figure 2.1, a simplified molecular orbital diagram, depicts the possible transitions in ethene. For ethene, the HOMO level is the π orbital and the LUMO level is the π^* orbital, respectively. [13, p. 564; 14, pp. 20–23] There are several vibrational energy

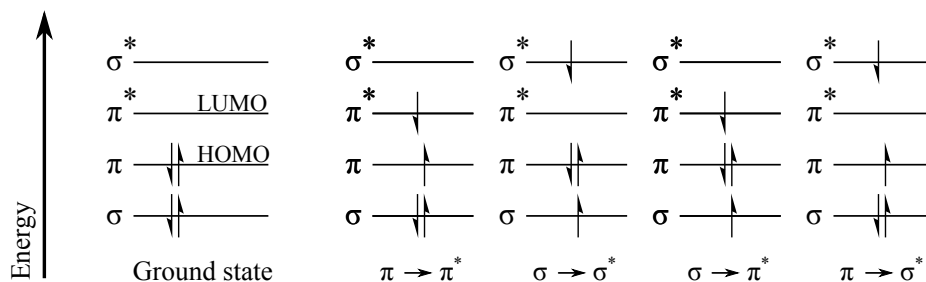


Figure 2.1. Electronic configuration of ethene molecule and the feasible electronic transitions. [14, p. 22]

levels within each electronic energy level. In Figure 2.1 the vibrational energy levels are omitted for clarity.

The required energy for a $\sigma \rightarrow \sigma^*$ transition is much larger than for a $\pi \rightarrow \pi^*$ transition, which can be seen in Figure 2.1. Usually the energies associated with different transitions are in the following order: [14, p. 21]

$$n \rightarrow \pi^* < \pi \rightarrow \pi^* < n \rightarrow \sigma^* < \sigma \rightarrow \pi^* < \sigma \rightarrow \sigma^* \quad (2.2)$$

The wavelengths corresponding to the $\sigma \rightarrow \sigma^*$ transition are located at the far ultraviolet region of the electromagnetic spectrum. The $n \rightarrow \pi^*$ and $\pi \rightarrow \pi^*$ transitions, on the contrary, are located at the visible part of the spectrum, which makes them easy to observe. [14, pp. 20–23]

For most compounds, however, the situation is not as simple as it is for ethene. This is why molecular orbital diagrams are usually not used for polyatomic molecules. Instead, one uses the concepts of ground state and (electronically) excited states in addition to the HOMO and LUMO levels.

The electron spin orientation is retained for all transitions presented in Figure 2.1. This means that the *total spin* of the molecule remains the same. The molecular spin arises from the spins of individual electrons. For the spin quantum number of an individual electron, m_s , there are two possible values: $m_s = +\frac{1}{2}$ or $-\frac{1}{2}$. The sum of the individual spins is denoted as M_S : $M_S = \sum m_s$. The sum of the individual electron spins is related to the total spin quantum number of the molecule, S : $M_S = -S, \dots, S$. In most molecules, all electrons are paired with opposite spins, and $S = 0$. Thus, in the transitions depicted in Figure 2.1, both the initial and the final state correspond purely to one state each, and the states are called *singlet states*. Singlet states of a molecule are commonly denoted as S_0 (the ground state), and S_1, S_2, \dots (the excited states). [13, pp. 469–478, 576; 14, pp. 20–23]

However, there is also a chance for a state with unpaired electrons. The sum of electron spin quantum numbers is then $M_S = -1, 0$ or 1 , which all correspond to $S = 1$. Such states, where one total spin quantum number corresponds to three different, isoenergetic states, are called *triplet states*, and denoted as T_1, T_2 , and so on. Usually, T_0 is not used, because a triplet state rarely is the ground state of a molecule. [13, pp. 469–478; 14, pp. 20–23] However, a famous exception is the oxygen molecule, whose ground state is a triplet state [13, p. 579; 15, p. 12].

The quantum mechanical selection rules state that transitions from a singlet state to a triplet state, or vice versa, are forbidden. In practice, however, there is a small but non-negligible probability for such a transition. This probability originates from the spin-orbit coupling, due to which the wave functions of the singlet and triplet states have some interaction. [14, p. 30; 16, pp. 316–317]

According to the Born–Oppenheimer approximation, the movement of electrons is much faster than that of the nuclei. This leads to the fact that the nuclei don't have time to move while the electron is promoted into a higher energy level. Therefore, the theoretical consideration of electronic transitions is simplified a lot by assuming that the nuclear conformation of the atoms in a molecule does not change in an excitation process. This assumption is called the Franck–Condon principle. [14, pp. 30–32; 17, p. 3–5] The situation is depicted in Figure 2.2. Since the nuclear configuration does not change, the most probable transition is depicted in Figure 2.2 with a vertical arrow. Thus, the transition is called a *vertical transition*. [14, p. 31; 18, pp. 387–391] The most probable transition seldom is the 0 – 0 transition (i.e. transition from the lowest vibrational level of the ground state to the lowest vibrational level of the excited state). Usually, the nuclear configurations of the ground and excited states are somewhat different, depicted by the different position of the potential energy curve minima in Figure 2.2. Thus, the vertical transition brings the electron to a higher-lying vibrational level of the excited state, as depicted in the figure. [18, pp. 386–389]

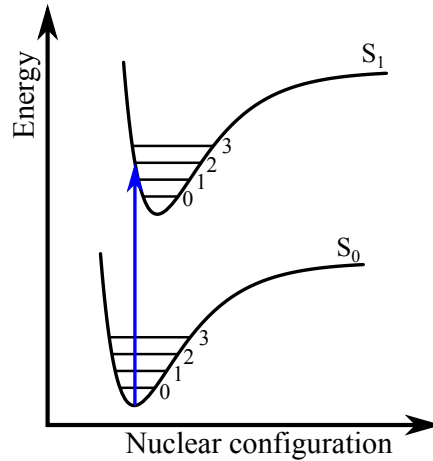


Figure 2.2. Potential energy curves for the ground state and the first singlet excited state of a molecule. The numbers denote the vibrational levels within the electronic energy levels. The transition from S_0 to S_1 is vertical. [14, p. 32]

2.1.2 Absorption in a bulk medium

When considering absorption in a bulk medium, instead of one molecule, we can handle measurable properties and derive laws concerning the absorption process.

Let light enter an isotropic, dielectric medium of thickness l , propagating along the x -axis of the coordinate system. Intensity of the light at some point in the medium is denoted with $I(x)$. During the propagation through a thin layer inside the medium of thickness $x + \Delta x$, the intensity is changed by ΔI . Thus, intensity at point $x + \Delta x$ is $I(x + \Delta x) = I(x) + \Delta I$. [15, pp. 1–6] The process is illustrated in Figure 2.3.

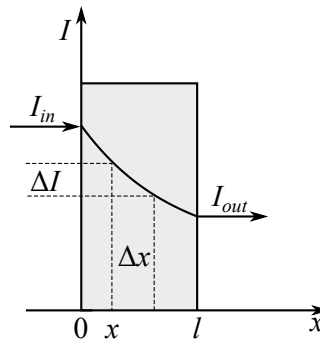


Figure 2.3. Absorption of light in an isotropic, dielectric medium. [15, p. 2]

When the thickness of the layer Δx approaches zero, the relative change in intensity is proportional to the intensity at x by the *absorption coefficient*, α : [15, pp. 1–6]

$$\lim_{\Delta x \rightarrow 0} \frac{\Delta I(x, \Delta x)}{\Delta x} = -\alpha I(x), \quad (2.3)$$

or, as a differential equation,

$$\frac{dI(x)}{dx} = -\alpha I(x). \quad (2.4)$$

Equation 2.4 can be rearranged as

$$\frac{dI(x)}{I(x)} = -\alpha dx. \quad (2.5)$$

This equation is easily solved by integration over the thickness of some layer in the medium, say, from 0 to x :

$$\ln \frac{I(x)}{I(0)} = -\alpha x. \quad (2.6)$$

Equation 2.6 can be converted to the exponential form:

$$I(x) = I(0) e^{-\alpha x}. \quad (2.7)$$

Equation 2.7 is known as the Lambert law. For convenience, let us denote the intensity of the light entering the absorbing medium, or $I(0)$, as I_{in} , and the intensity of the light leaving the absorbing medium, or $I(x = l)$, as I_{out} , respectively. [15, pp. 1–6] Thus, intensity of the light after an absorbing medium of thickness l is

$$I_{out} = I_{in} e^{-\alpha l}. \quad (2.8)$$

The *transmittance* of the sample, T , is defined as [15, p. 3]

$$T = \frac{I_{out}}{I_{in}} = e^{-\alpha l}. \quad (2.9)$$

As can be seen from Equation 2.9, transmittance describes the relative amount of the light passing through the sample.

Mostly due to historical reasons, the power of 10 rather than the power of e is often used [15, pp. 1–6]. With this notation, Equation 2.8 is transformed to

$$I_{out} = I_{in} 10^{-A}, \quad (2.10)$$

where A is called the *absorbance*, or sometimes the *optical density*. [15, pp. 1–6] Equation 2.10 can be solved for the absorbance, resulting in a relation between the absorbance and transmittance:

$$A = -\log \frac{I_{out}}{I_{in}} = -\log T. \quad (2.11)$$

In practical work, it is often convenient to relate the absorbance of a sample to the density and the absorption efficiency of the chromophores (the absorbing species). For samples in solution, this is achieved with the Beer–Lambert law: [15, p. 4]

$$A = \varepsilon cl, \quad (2.12)$$

where c is the concentration of the absorbing species in the sample solution (in mol dm⁻³, or M), l is the thickness of the sample, or optical path length (in cm, for historical reasons), and the proportionality coefficient ε is called the *molar absorption coefficient*. Since absorbance is a dimensionless quantity, ε is measured in M⁻¹ cm⁻¹. [15, pp. 1–6]

2.2 Relaxation of the excited state

Since the excited state is energetically less favourable than the ground state, the excited electron inevitably returns back to the ground state at some point. This process is referred to as *relaxation* of the excited state. In the following Sections, the different relaxation mechanisms are described shortly. Some important quantities concerning the relaxation processes are derived.

2.2.1 Relaxation mechanisms of the excited state

The different relaxation mechanisms are depicted in Figure 2.4, the Jablonski diagram for an arbitrary molecule [14, p. 34–37]. The diagram was named after its inventor Alexander Jablonski (1898 – 1980) [17, p. 4–5]. In the diagram, the heavy horizontal lines depict the different electronic states, and the light horizontal lines show schematically the various vibrational levels within each electronic state. The arrows indicate the transitions between the states. [14, pp. 34–37]

Let us have a look at the different relaxation mechanisms. The transitions can be divided into two categories, namely radiative transitions (represented by the straight arrows in the Jablonski diagram), and non-radiative transitions (represented by the wavy arrows in the diagram). The radiative processes (involving a photon) include fluorescence and phosphorescence, in addition to absorption, whereas the non-radiative processes are internal conversion (IC), intersystem crossing (ISC), and vibrational relaxation (VR). [13, pp. 955–964; 14, pp. 37–42]

Vibrational relaxation

Strictly speaking, vibrational relaxation is not a real photochemical process. However, in solution it is often coupled with the other relaxation mechanisms, leading the molecule towards the lowest vibrational level of an electronic state. Vibrational

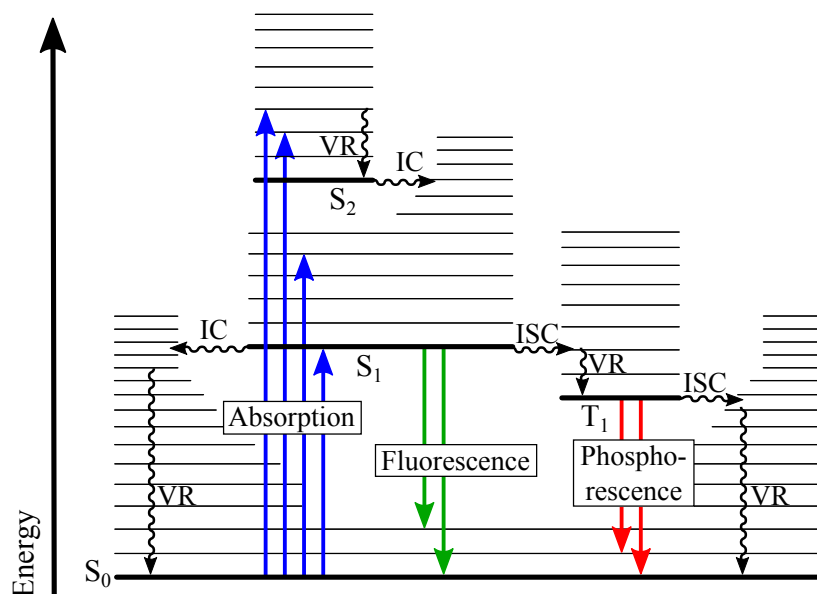


Figure 2.4. Jablonski diagram. [14, p. 35]

relaxation originates from collisions of the vibrationally excited molecule with solvent molecules. In these collisions, energy is transferred from the excited molecule to the solvent molecules, and the molecule is relaxed to the lowest vibrational level of the electronic state. The time required for the vibrational relaxation is short compared to the timescale of the other relaxation processes, and therefore all other relaxations usually start from the lowest vibrational level of an electronic state. [13, pp. 955–964; 14, pp. 37–42]

Internal conversion

According to the International Union of Pure and Applied Chemistry (IUPAC) [19], internal conversion is “an isoenergetic radiationless transition between two electronic states of the same multiplicity”. Usually the final state is a high-lying vibrational level of a lower electronic state, and the molecule is said to be *vibrationally hot*. Internal conversion is practically always followed by a very fast vibrational relaxation towards the lowest vibrational level of the final state. The rate of internal conversion depends on the energy difference of the initial and final electronic states. If the energy difference is small, the relaxation is very fast. On the contrary, if the energy difference is large (e.g. S_1 vs. S_0), the internal conversion is slower. The slower rate leads to a smaller probability for the internal conversion, since other relaxation mechanisms like fluorescence and intersystem crossing compete with it. [13, pp. 955–964; 14, pp. 37–42; 17, pp. 3–5]

Fluorescence

Fluorescence is the most significant relaxation mechanism concerning this Thesis. It is the radiative transition from an excited state to some of the vibrational levels of S_0 , followed by rapid vibrational relaxation to the lowest vibrational level of the ground state. In most cases, the transition is initiated from the lowest vibrational level of S_1 state. Energy of the emitted photon depends on onto which vibrational level the molecule returns. [14, pp. 37–38] Because of vibrational relaxation at the initial state, there is always energy loss, and the wavelengths of the emitted photons are longer than those of the absorbed photons. This phenomenon was first published by Sir George Gabriel Stokes in 1852, and thus it referred to as the Stokes law. [17, pp. 5–7; 20] However, Stokes’s formulation was only based on empirical observations, and the explanation for the phenomenon was discovered later.

The spacings between the vibrational levels are (almost) equal in the ground state and the first singlet excited state. This is why the lowest-energy band of the absorption spectrum (corresponding to $S_0 \rightarrow S_1$ transition) and emission spectrum are mirror images of each other. The difference between the positions of the absorption and emission maxima is called the *Stokes shift*, and it is often measured in terms of wavelength (in nm) or *wave number*, $\bar{\nu} = \lambda^{-1}$ (in cm^{-1}). [14, pp. 37–42] A typical Stokes shift for a molecule is below 10 nm. For example, Rhodamine 6G has a large Stokes shift of 25 nm. [15, pp. 116–117] The absorption and emission spectra of Rhodamine 6G are shown with the Stokes shift in Figure 2.5, together with the structure of the compound.

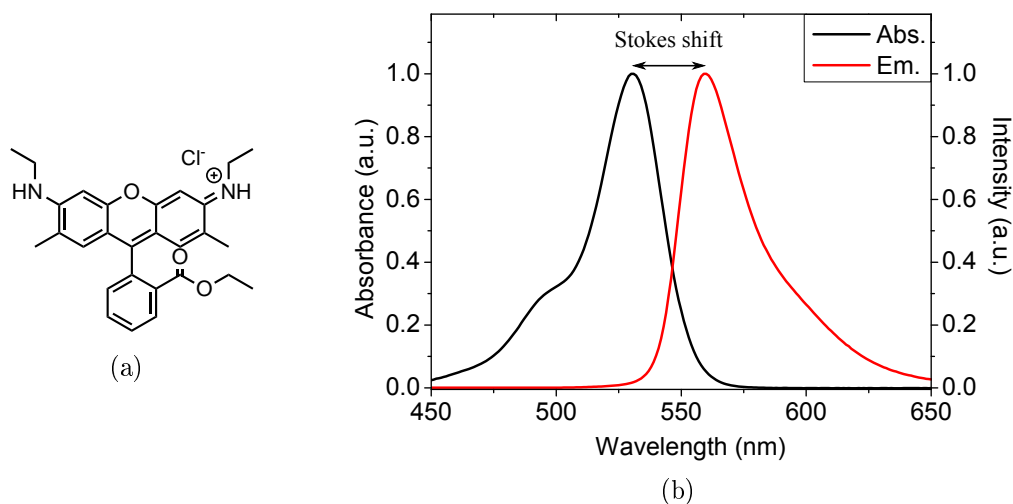


Figure 2.5. (a) Molecular structure, and (b) absorption and emission spectra for the fluorescent dye Rhodamine 6G.

The timescale for emitting a photon is as fast as absorption, which is extremely fast compared to all the other processes. However, the molecule does spend some

time (up to a few hundred nanoseconds) in the excited state before relaxing back to the ground state. [14, pp. 37–38]

Intersystem crossing

There is a small probability for a transition from a singlet state to a triplet state, as discussed in Section 2.1.1. Such a transition where the spin multiplicity changes is called an intersystem crossing. Most often, intersystem crossing occurs from the first singlet excited state (S_1) to some vibrational level of a close-lying triplet state, or from a triplet state to a lower-lying singlet state. [14, pp. 37–42] Just like internal conversion, intersystem crossing is a non-radiative process resulting in a vibrationally hot molecule on the final state.

Phosphorescence

Phosphorescence is the triplet–singlet counterpart for fluorescence, i.e. it is the radiative transition from the a triplet state to some vibrational level of a lower-lying singlet state, usually $T_1 \rightarrow S_0$. Because a triplet-singlet transition is forbidden considering the selection rules, the probability for the transition is very low. Usually, phosphorescence is difficult to observe in solutions because it competes with numerous different relaxation pathways, e.g. intersystem crossing to S_1 and triplet–triplet annihilation. [14, pp. 41–42; 17, p. 1–5]

2.2.2 Quantum yields and lifetimes

Let us consider a dilute solution of a fluorescent species. For simplicity, let us assume only two electronic states, S_0 and S_1 , and discard vibrational relaxation processes, which would complicate the reaction kinetics. Let us denote the concentration of the species in the excited state with $[S_1]$. Following the notation of classical chemical kinetics, the differential rate law for disappearance of S_1 is written [13, p. 959; 14, pp. 42–43]

$$-\frac{d[S_1]}{dt} = (k_r^S + k_{nr}^S)[S_1], \quad (2.13)$$

where the proportionality coefficient $k_r^S + k_{nr}^S$ is the sum of the radiative and non-radiative *rate constants* for the relaxation of the S_1 state. As discussed earlier, fluorescence is the radiative relaxation pathway from the S_1 state, so k_r^S is the rate constant for fluorescence. The non-radiative constant k_{nr}^S , on the other hand, includes all non-radiative relaxation pathways from S_1 , namely internal conversion, and intersystem crossing from S_1 to a triplet state, T_1 . Thus, $k_{nr}^S = k_{IC}^S + k_{ISC}^S$. [14, p. 42]

Equation 2.13 can be solved by integration:

$$[S_1] = [S_1]_0 e^{-(k_r^S + k_{nr}^S)t}, \quad (2.14)$$

where $[S_1]$ is the concentration of the excited molecules at time t , and $[S_1]_0$ the concentration at $t = 0$, respectively. Let us define τ_S , the *lifetime* of the excited state, as [14, p. 43]

$$\tau_S = (k_r^S + k_{nr}^S)^{-1}. \quad (2.15)$$

With this notation, Equation 2.14 is written as

$$[S_1] = [S_1]_0 e^{-\frac{t}{\tau_S}}. \quad (2.16)$$

Thus, after one lifetime, concentration of the excited molecules has dropped to e^{-1} of that of the original concentration. If fluorescence is much faster than the non-radiative processes, i.e. $k_r^S \gg k_{nr}^S$, then $\tau_S \approx (k_r^S)^{-1}$ [13, pp. 955–964]. It is important to notice that the lifetime describes the average time the molecule spends in the excited state *before* emitting a photon or relaxing by some non-radiative mechanism. The relaxation itself is extremely fast, regardless of the mechanism. [14, p. 38]

Usually, emission intensity is measured instead of concentration. At any time t , the fluorescence intensity I_F is proportional to the concentration of the molecules:

$$I_F = k_r^S [S_1] = k_r^S [S_1]_0 e^{-\frac{t}{\tau_S}}, \quad (2.17)$$

where the proportionality factor is the rate constant for fluorescence [14, pp. 43–44].

Let us define another useful quantity that describes the relative efficiency of a process in terms of the number of photons, the *quantum yield*. Quantum yield for any photo-initiated process i is defined as [19]

$$\Phi_i = \frac{\text{number of events}}{\text{number of absorbed photons}}. \quad (2.18)$$

Since every absorbed photon produces an excited molecule, and every excited molecule must relax by some pathway with a corresponding rate constant, the quantum yield can also be written as [21, p. 208]

$$\Phi_i = \frac{k_i}{\sum_j k_j}, \quad (2.19)$$

where k_i is the rate constant of the process under observation, and $\sum_j k_j$ is the sum of all rate constants leading away from the initial state. For example, for fluorescence

the quantum yield is [14, p. 46]

$$\Phi_{\text{F}} = \frac{k_{\text{r}}^{\text{S}}}{k_{\text{r}}^{\text{S}} + k_{\text{nr}}^{\text{S}}} = k_{\text{r}}^{\text{S}} \tau_{\text{S}}, \quad (2.20)$$

where τ_{S} is the lifetime of the excited state defined in Equation 2.15.

Similar derivation can be carried out for the triplet state. Then, the rate law for the disappearance of the triplet state is [14, pp. 45–46]

$$[\text{T}_1] = [\text{T}_1]_0 e^{-\frac{t}{\tau_{\text{T}}}}, \quad (2.21)$$

where τ_{T} is the lifetime of the triplet state, $\tau_{\text{T}} = (k_{\text{r}}^{\text{T}} + k_{\text{nr}}^{\text{T}})^{-1}$. The radiative rate constant for the triplet state is actually the rate constant for phosphorescence, and the non-radiative rate constant consists of contributions from all non-radiative relaxation pathways, such as the intersystem crossing from T_1 back to S_0 , and triplet–triplet annihilation. [14, pp. 41–42] A quantum yield can also be derived for phosphorescence: [14, p. 46]

$$\Phi_{\text{P}} = \frac{k_{\text{r}}^{\text{T}}}{k_{\text{r}}^{\text{T}} + k_{\text{nr}}^{\text{T}}} = k_{\text{r}}^{\text{T}} \tau_{\text{T}}. \quad (2.22)$$

However, since only some of the excited molecules undergo an intersystem crossing to the T_1 state, the efficiency of this process has to be taken into account: [14, p. 46]

$$\Phi_{\text{P}} = \Phi_{\text{ISC}} \frac{k_{\text{r}}^{\text{T}}}{k_{\text{r}}^{\text{T}} + k_{\text{nr}}^{\text{T}}} = \Phi_{\text{ISC}} k_{\text{r}}^{\text{T}} \tau_{\text{T}}, \quad (2.23)$$

where Φ_{ISC} is the quantum yield for intersystem crossing, $\Phi_{\text{ISC}} = k_{\text{ISC}} \tau_{\text{S}}$. [14, p. 46]

Phosphorescence quantum yields are generally lower than for fluorescence. Firstly, not all excited molecules reach the triplet state, so usually the quantum yield for intersystem crossing is less than unity. Secondly, as discussed in Section 2.2.1, phosphorescence competes with several other relaxation processes. However, lifetimes for phosphorescence are long, extending even to seconds, because the probability for the transition back to S_0 is also low due to the selection rules. [14, p. 46; 17, p. 1]

2.3 Excited-state intramolecular proton transfer

Sometimes the excitation induces also chemical reactions, in addition to the photophysical processes described previously. The most simple chemical reactions of all are electron transfer and proton transfer. In this Thesis, the excited state intramolecular proton transfer (ESIPT) process is discussed.

2.3.1 Proton transfer compounds

The most crucial requirement for a proton transfer happening intramolecularly is the presence of a proton donor and a proton acceptor in the molecule, and the formation of an intramolecular hydrogen bond between them. Usually, the proton donor is a hydroxyl group or an amino group, and the acceptor a carbonyl group or a pyridyl nitrogen. Figure 2.6 shows some examples of the molecules undergoing an ES IPT: methyl salicylate (MS), 5-(2-pyridyl)-1-H-pyrazole (PP), and 10-hydroxybenzo[*h*]quinoline (HBQ). [2; 5, p. 238–242] In the figure, the dashed bonds represent the intramolecular hydrogen bonds.

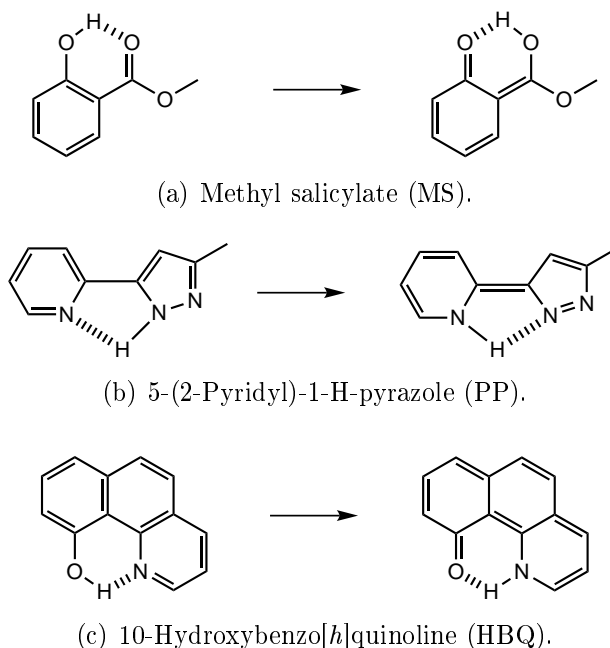


Figure 2.6. Molecules undergoing excited-state intramolecular proton transfer [2, 5].

In all these compounds, the proton donor–acceptor pairs are different. In methyl salicylate, a hydroxyl group serves as the donor and carbonyl oxygen is the acceptor, whereas in 5-(2-pyridyl)-1-H-pyrazole, the donor is the pyrazole moiety of the molecule with some amino character, and the acceptor is a pyridyl nitrogen [2; 5, p. 238]. In 10-hydroxybenzo[*h*]quinoline, the donor is again a phenolic hydroxyl group, and the adjacent pyridine moiety serves as the proton acceptor. [5, pp. 238–242]

The compounds in Figure 2.6 differ from each other not only in the type of the proton donor and acceptor, but also in the size of the intramolecular hydrogen bond ring. In MS and HBQ the intramolecular hydrogen bond participates in a six-membered ring structure, whereas in PP the ring is only five-membered, and the structure is thus more strained. In fact, bending of the molecule is needed for

the ESIPT to occur. [2; 5, p. 239–246] In HBQ, geometry of the molecule is very restricted, so the proton donor and acceptor are forced into optimal distance and orientation for the intramolecular hydrogen bond. Thus, the hydrogen bond is very strong. [5, p. 242] However, in all cases the donor and acceptor need to be in close proximity for the proton transfer to occur.

2.3.2 Proton transfer reaction

The most distinctive property of a compound undergoing an ESIPT is its fluorescence. In the ground state, the molecule is in its “normal” tautomer form (on the left in Figure 2.6). When it is excited, however, the proton is transferred from the donor to the acceptor, resulting in the excited state of the “proton-transfer” tautomer (on the right in Figure 2.6). This excited state then relaxes to the ground state of the proton-transfer tautomer by fluorescence. However, since the excited state of the proton-transfer tautomer lies lower in energy, and the ground state energy is larger than that of the normal tautomer, wavelength of the emitted photons is much longer than for the emission of the normal tautomer. Thus, the Stokes shifts of the ESIPT molecules are anomalously large. Since the ground state of the proton transfer tautomer lies higher in energy than the normal tautomer, the proton transfer tautomer relaxes back to the normal tautomer ground state by a non-radiative back proton transfer. [5, pp. 238–239]

Because the “normal” tautomer form is energetically more favourable in the ground state, the normal tautomer can also be called the ground state tautomer. For many compounds (HBQ and MS, for example), the ground state tautomer can be treated as an enol, so it is often called the enol tautomer. The proton-transfer tautomer is then called the keto tautomer, respectively.

Figure 2.7 depicts the proton transfer mechanisms in HBQ in a simplified way. In

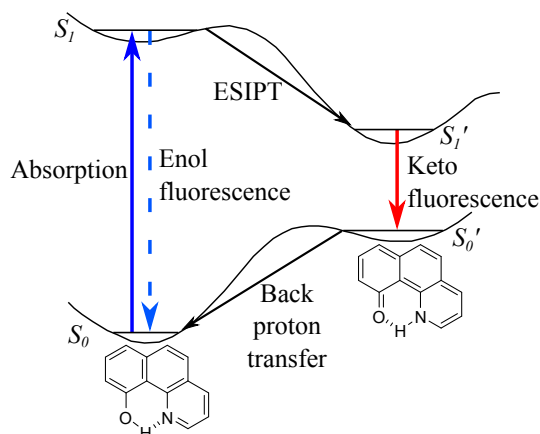


Figure 2.7. A simplified scheme of the energy profiles associated with the excited-state intramolecular proton transfer in HBQ. [5]

the figure, S_0 and S_1 refer to the ground state and the first singlet excited state of the enol tautomer, and S'_0 and S'_1 to the ground state and the first excited state of the keto tautomer, respectively. Hereafter, the prime sign always indicates the proton transfer tautomer. The solid lines with arrows depict the enol tautomer absorption and keto tautomer fluorescence. [5, p. 238] To some extent, the excited state of the enol tautomer, also called the *locally excited state*, relaxes directly back to its ground state, and there is a very weak enol tautomer fluorescence as well, depicted by the dashed arrow in Figure 2.7. Usually the proton transfer is so rapid that in steady-state measurements the enol tautomer fluorescence is not observed. For HBQ, the absorption maximum (in cyclohexane solution) is located at ca. 380 nm, and the (keto tautomer) emission is maximized at 635 nm. [9] Thus, the Stokes shift is enormous: 255 nm.

2.3.3 Reaction mechanism

The ESIPT process consists of two stages: the transfer of the proton and the electron. The relative rates of these stages determine the sensitivity of the proton transfer process towards solvent polarity, for example. According to the Franck–Condon principle, during the electronic excitation there is no nuclear movement. [22] However, once the molecule is in the S_1 state, there are two possibilities for the process to continue: the proton transfer and the electron transfer. The situation is depicted in Figure 2.8. The ESIPT molecule is illustrated with a benzene-like structure. D_e and A_e denote the electron donor and acceptor, and D_H and A_H the proton donor and acceptor, respectively. In ESIPT compounds in practice, the proton acceptor usually serves as the electron acceptor as well. [22]

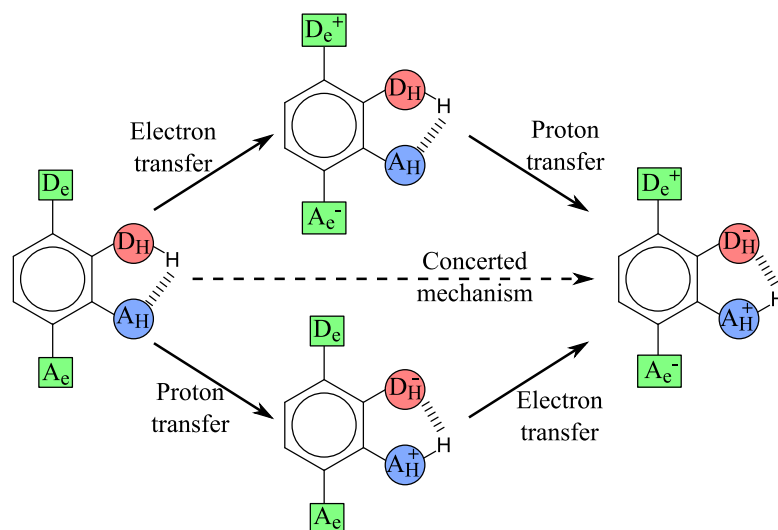


Figure 2.8. A general scheme of an ESIPT reaction. [22]

If the rate of electron transfer is sufficiently high, it precedes the proton transfer. This is illustrated by the upper reaction route in Figure 2.8. The electron transfer from D_e to A_e is extremely fast: it cannot be detected with the present instruments which have a detection limit of ~ 150 fs. Once the electron transfer is complete, it is followed by the proton transfer, as shown in Figure 2.8. These processes can be called “electron-coupled proton transfer”, and they comprise the majority of all ESIPT processes. [22]

The other possibility is the proton transfer followed by the electron transfer, depicted by the lower reaction route in Figure 2.8. This reaction route is possible because the hydrogen bonded H atom may possess a very strong photoacidic character upon excitation. Thus, the proton transfer can take place immediately after excitation. The latter case is less common among the ESIPT systems studied so far, but there are specially designed systems where this “proton-coupled electron transfer” can be investigated. The proton transfer and the electron transfer may also occur simultaneously. Then the mechanism is called *concerted*, depicted in Figure 2.8 by the dashed arrow in the middle. [22] Because the rate of the electron transfer is extremely fast, it is difficult to determine whether a process occurs via the proton-coupled electron transfer mechanism or via the concerted mechanism. [23]

As can be observed in Figure 2.8, the proton transfer is always accompanied with drastic changes in the electron density distribution and the dipole moment of the molecule. The charge differences generated in the electron transfer / proton transfer process quickly cancel out as the proton is transferred. For example, the electron density change in HBQ is schematically illustrated in Figure 2.9. [11] The arrows depict the movement of an electron pair.

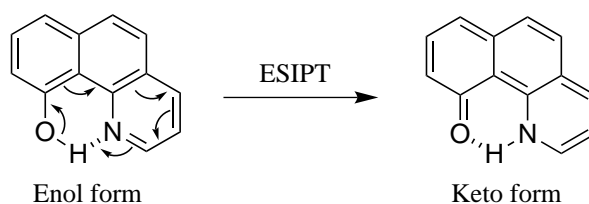


Figure 2.9. Electron density redistribution during the ESIPT in HBQ. [11]

Strictly speaking, the process discussed so far is a hydrogen atom transfer rather than a proton transfer, because both the proton and the electron are transferred, and the covalent bond between the hydrogen atom and the hydrogen donor is broken. According to Zewail *et al.* [2], only a process which leads to a zwitterionic species and which does not require redistribution of the electron density should be called a proton transfer. Thus, the reaction product for a “pure” proton transfer would be the

intermediate species in the proton-coupled electron transfer mechanism (depicted by the lower reaction route in Figure 2.8). However, the term “proton transfer” is widely used in literature to describe the whole process depicted in Figure 2.8, and thus it is used in this Thesis as well.

2.3.4 Substituent effects

Since the number of different compounds capable of ESIPT is so vast, it is practically impossible to make any general conclusions about the effect of different substituents. However, since this Thesis is devoted to HBQ derivatives, some statements on the substituent effect in HBQ are given.

As discussed earlier in Section 2.3.3, the electronic configurations for the ground state and proton transfer tautomers are quite different in any ESIPT molecule. In HBQ, the HOMO and LUMO levels of the enol tautomer are delocalized over the whole π electron network, as is expected for any aromatic compound. However, in the keto tautomer, the situation is totally different. According to Chou *et al.* [11], the HOMO level of the keto tautomer is located at the cyclohexa-2,4-dienone moiety, whereas the LUMO level is located at the methylenepyridine moiety. The location of the HOMO and LUMO levels is depicted in Figure 2.10. In the figure, the HOMO level of the keto tautomer is located on the left-hand side of the molecule, and the LUMO level on the right-hand side, respectively. [11]

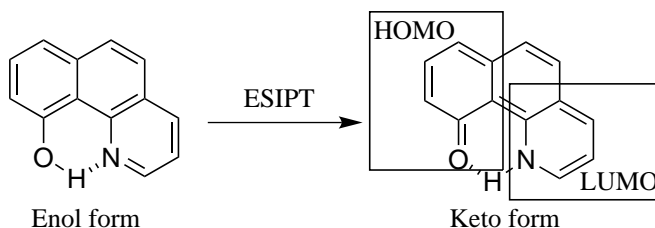


Figure 2.10. HOMO and LUMO levels of the keto tautomer of HBQ are located on different parts of the molecule. [11]

The enol tautomer of a HBQ derivative is not expected to experience a great substituent effect, because substituting the HBQ core with different functional groups perturbs the HOMO and LUMO levels simultaneously. Thus, the energy difference between HOMO and LUMO does not change. Since the enol tautomer can be detected mainly by absorption spectroscopy, the absorption spectra of differently substituted HBQ derivatives are quite similar. [11]

The situation is quite different in the keto tautomer because of the different localization of the HOMO and LUMO levels. For example, when substituting the cyclohexa-2,4-dienone part of the molecule with electron-withdrawing groups, the

energy of the HOMO level is decreased. This leads to an increase in the energy gap between the HOMO and LUMO levels of the keto tautomer. Then, fluorescence band of the keto tautomer, corresponding to transition from S'_1 to S'_0 , is shifted to shorter wavelengths. On the contrary, on substituting an electron-donating group on the same part of the molecule, the energy of HOMO level is increased, and the corresponding fluorescence emission is shifted to longer wavelengths. [11]

Similarly, substituting the methylenepyridine moiety with an electron-donating group leads to shorter emission wavelengths due to an increase in the LUMO energy, and substituting the same moiety with an electron-withdrawing group leads to longer emission wavelengths due to a decrease in the LUMO energy. [11]

2.3.5 Solvent effects

In non-polar solvents, interaction with the intramolecular hydrogen bond and the solvent is minimal. However, solvent relaxation always makes the reaction kinetics more complicated. When increasing the solvent polarity, the solvent interacts more with the intramolecular hydrogen bond. Whether the overall reaction rate is increased or decreased with increasing solvent polarity is determined by the relative rates of proton and electron transfer.

In ES IPT systems where the electron transfer precedes the proton transfer, the proton transfer competes with solvent relaxation associated with the electron-transfer tautomer, i.e. the process $S_1^{\text{ET}} \rightarrow S_{1\text{eq}}^{\text{ET}}$. Once the equilibrium between the electron-transfer tautomer and the solvent has been achieved, the dipole moment of $S_{1\text{eq}}^{\text{ET}}$ may be significantly larger (in magnitude) than that of $S'_{1\text{eq}}$. This leads to a solvent-induced energy barrier for the ES IPT reaction. [22] When the solvent polarity is increased, the ground state tautomer possessing the larger dipole moment is stabilized by the solvent, which reduces the overall proton transfer rate and prolongs the fluorescence lifetimes. [22, 23] For example, in 4'-*N,N*-diethylamino-3-hydroxyflavone (3HF), the proton transfer rate is reduced by 15 times when changing from the non-polar cyclohexane to the polar acetonitrile [24]. Structure of 3HF is presented in Figure 2.11(a).

As already mentioned in Section 2.3.3, in vast majority of the systems studied so far, the ES IPT occurs via the electron-coupled proton transfer mechanism. Since the early dynamics of this process are always perturbed by the solvent relaxation, there is a great interest in finding a system free from the solvent relaxation interference. [22] The ideal systems for this purpose use the proton-coupled electron transfer mechanism, where the proton transfer occurs before the electron transfer, or the concerted mechanism with simultaneous proton and electron transfer. [23] When exciting a molecule of this type, the proton transfer tautomer in its excited state (S'_1) may possess much larger dipole moment than the locally excited state.

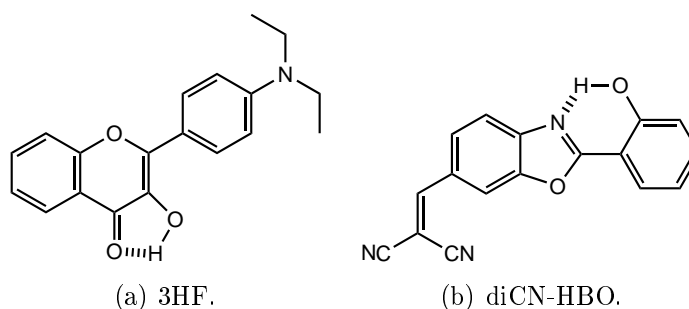


Figure 2.11. Structures of (a) 4'-N,N-diethylamino-3-hydroxyflavone (3HF) and (b) 2-[[2-(2-hydroxyphenyl)benzo[d]oxazol-6-yl]methylene]malononitrile (diCN-HBO). [22]

Because the proton transfer reaction is involved with such a drastic change in the dipole moment, the reaction dynamics are directly dependent on solvent relaxation, which leads to a solvent-induced energy barrier. [22, 23] When the solvent polarity is increased, the proton transfer tautomer is stabilized by the solvent more than the ground state tautomer, so that the solvent-induced barrier is decreased, and an increase in the overall reaction rate is expected. In other words, the energy minimum associated with the solvent relaxation of S'_1 is reduced with increasing solvent polarity, which leads to faster ESIP T and shorter fluorescence lifetimes. [23] There are some carefully designed systems for the concerted ESIP T mechanism, 2-[[2-(2-hydroxyphenyl)benzo[d]oxazol-6-yl]methylene]malononitrile (diCN-HBO), for example. The structure of diCN-HBO is presented in Figure 2.11(b). In this system, the proton transfer rate has been reported to increase by 3.5 times when measured in the polar acetonitrile compared to the non-polar cyclohexane. [22, 23]

The previous discussion concerned only non-polar and polar aprotic solvents. However, in protic solvents the situation is quite different. For most compounds, the solvent perturbation on the intramolecular hydrogen bond is significant. The proton transfer rate is then either greatly reduced, or there is a total lack of proton transfer, and only normal emission is observed. [22, 25] In the latter case, the intramolecular hydrogen bond is broken by the solvent perturbation and it is replaced with an intermolecular hydrogen bond between the solute and solvent. Thus, the solvent perturbation makes the reaction kinetics even more complicated than in aprotic solvents. [12, 22]

However, there are systems in which the proton transfer in protic solvents can be investigated. There are two possibilities for constructing such a system: either, the intramolecular hydrogen bond must be so strong that the proton transfer reaction remains unaffected even in protic solvents, or the solvent must assist in the proton transfer.

An example of the former case is HBQ. The geometrically restricted structure forces the hydroxyl oxygen and benzoquinolinic nitrogen in so close proximity that

the intramolecular hydrogen bond is very strong, ~ 10 kcal mol $^{-1}$, compared to the commonly measured < 8 kcal mol $^{-1}$ [26, see 12]. Thus, even in alcohols or water, HBQ undergoes the proton transfer reaction, and dual emission consisting of both the enol tautomer and keto tautomer emissions is observed. The intensity ratio between the two emission bands depends on the pH [12]. It has been concluded that, in aqueous solutions, the driving force for the proton transfer reaction in HBQ is the resonance charge transfer between the oxygen and the nitrogen in the excited state, rather than the intramolecular hydrogen bond itself [5, pp. 243–244; 12].

Excited-state intramolecular proton transfer processes can also be studied with specially designed compounds that intrinsically lack any intramolecular hydrogen bond, but can produce one either by self-dimerization or by assistance of the protic solvent molecules [22]. The solvent-assisted proton transfer can only occur in protic solvents like water or alcohols. An example of a compound undergoing this kind of proton transfer is 7-azaindole, for which both the self-dimerization and the solvent-assisted proton transfers are possible. [27–29] Both processes are depicted in Figure 2.12.

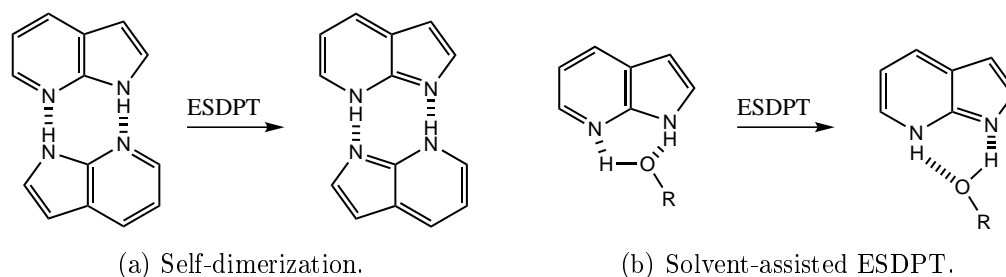


Figure 2.12. Excited-state double proton transfer in 7-azaindole can occur either by (a) self-dimerization or by (b) assistance of the solvent. [28]

As can be observed in Figure 2.12, there is no possibility for an intramolecular hydrogen bond in the molecule. Proton transfer can only occur via one of the two mechanisms depicted in the figure. In fact, in both processes, two protons are exchanged, so the processes can be called excited-state double proton transfer (ESDPT) [22].

2.3.6 Possible applications

Excited-state proton transfer reactions provide a means to mimic many biological systems. For example, 7-azaindole can be used to model the DNA base pair adenine–thymine because of the similar structure at the hydrogen-bonding area. Studying the proton transfer in this kind of systems is important, since proton transfer in DNA may cause mutations. Per-Olov Löwdin suggested in 1965 [30], that proton transfer along the DNA chain produces “tautomeric” base pairs, which

pair differently than the original base pairs. Then, in the next duplication, the genetic information is erroneous, i.e. there is a mutation. Thus, investigating the photoinduced proton transfer in 7-azaindole, a deeper understanding of the dynamics of mutagenesis in DNA can be achieved. [27]

Another very important application for ESIPT compounds in the field of biology and biochemistry is fluorescence probing. For example, relaxation dynamics of protein molecules in a solution, or the structural stability of the protein binding site, can be monitored with the fluorescence of the proton-transfer tautomer [7, 31]. Furthermore, fluorescence probes insensitive to solvent relaxation can reveal information on the structural transitions in biopolymers, e.g. folding and unfolding of a protein. HBQ has been suggested as a fluorescence probe for such applications. [6]

The solvent-assisted ESIPT process is also involved with the fluorescence of Green Fluorescent Protein, GFP. GFP has numerous applications in biochemistry and medicine as a cell marker with which one can detect the activities within living cells. In 2008, Osamu Shimomura, Martin Chalfie, and Roger Tsien were awarded the Nobel Prize in Chemistry for the discovery and development of GFP. [5, 32]

In addition to biological applications, ESIPT compounds can be utilized in other fields as well. Since the invention of the organic light-emitting diode (OLED) and the early work of Tang and VanSlyke, *et al.*, and Burroughes *et al.*, for example [33, 34], the research on the field has been growing explosively. The usage of ESIPT compounds with high fluorescence quantum yields and large Stokes shifts without self-absorption has been promising for OLED applications, especially for white-emitting devices. White OLEDs, or WOLEDs, intrigue many researchers, since they could serve as the backlight unit for liquid crystal displays (LCD), and could also be used in future lighting applications. [35]

Another application worth to mention are dye lasers. Properties of ESIPT compounds are very beneficial for lasing applications, avoiding some of the major drawbacks in the conventional laser dyes [10, 36–38]. The four separate electronic states and the ultrafast enol–keto tautomerization enable easy and efficient population inversion. Furthermore, the initial concentration of the keto tautomer ground state is zero, and it also remains low because of the fast back proton transfer. Thus, the ESIPT compounds are very photostable in lasing applications [10, 37]. The extremely large Stokes shifts ensure a low self-absorption, which together with relatively high keto tautomer fluorescence quantum yields enables a high gain [37].

3 RESEARCH METHODS AND MATERIALS

The measurements were carried out at the Department of Chemistry and Bioengineering, at Tampere University of Technology, during summer and autumn 2011. The following Sections provide short descriptions of the instruments used as well as list the materials used in this work.

3.1 Measurement methods

The ESIPT processes were studied with steady-state as well as time-resolved methods. Steady-state measurement methods include absorption and emission spectroscopy. The sample is continuously illuminated, and the absorbance or emission intensity is monitored as a function of wavelength. In time-resolved emission spectroscopy, the fluorescence emission of the sample is monitored at a fixed wavelength as a function of time.

3.1.1 Steady-state spectroscopy

In this Thesis, absorption spectroscopy is used to determine the absorption efficiency of the samples at different wavelengths in order to check sample characteristics, and fluorescence emission spectroscopy is used to investigate the efficiency of the ESIPT reaction in the samples. Both methods are also used for planning other measurements.

Absorption spectroscopy

Measurement of the absorption spectrum for a compound is a common procedure in various fields, and it often precedes other measurements. A commercial instrument for measuring the absorption spectrum is commonly called a *spectrophotometer*. [15, p. 89] There are many different kinds of spectrophotometers available, and only the key aspects considering the instruments are discussed here.

In order to know the absorption efficiency of a sample, one must pass a beam of light through the sample and measure the light intensities before and after the sample (I_{in} and I_{out} , as defined in Section 2.1.2). Then, the quantities of interest, e.g. absorbance or transmittance, can be calculated. The absorption depends on wavelength, so the measurement needs to be carried out using a monochromatic

light source and repeated at different wavelengths in small steps along the desired wavelength range. To achieve this, a light source and a monochromator are needed. In addition, a detector is needed to measure the light intensity. The detector is often a photomultiplier tube, so the detected signal is actually the photomultiplier output voltage U , proportional to the light intensity: $U = sI$. The proportionality factor s is the *voltage sensitivity* of the detector. In order to measure the absorption of the sample, one must carry out two measurements. Without the sample, the output voltage is $U_1 = sI_{in}$, and with the sample, $U_2 = sI_{out}$. [15, pp. 89–92] Thus, the ratio of intensities is given by [15, p. 90]

$$\frac{U_2}{U_1} = \frac{I_{out}}{I_{in}}. \quad (3.1)$$

The intensity of the light depends on the wavelength, so actually $U = U(\lambda)$.

There are two main types of spectrophotometers: one channel and two channel instruments. One channel instruments suffer from some major drawbacks, such as more time-consuming measurements and sensitivity to thermal fluctuations, so only two channel instruments are discussed here. [15, pp. 92–95] Figure 3.1 gives a schematic view of a two channel spectrophotometer.

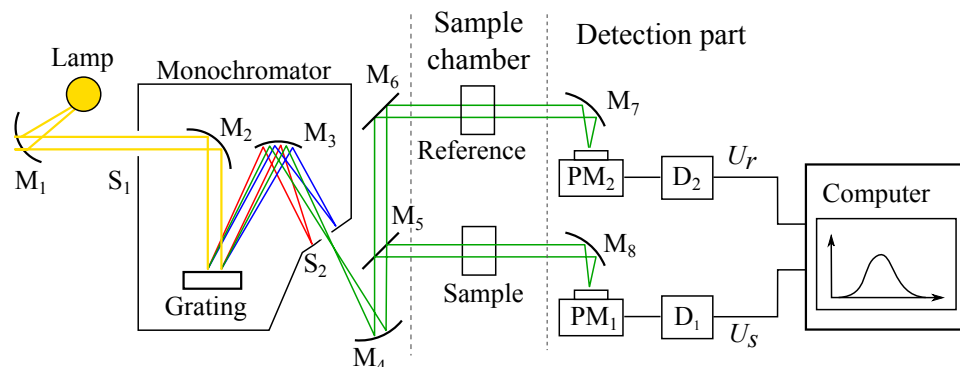


Figure 3.1. Schematic view of a two channel absorption spectrophotometer. S_1 and S_2 are the input and output slits of the monochromator, $M_1 - M_8$ are mirrors, PM_1 and PM_2 photomultipliers for each channel, and D_1 and D_2 the corresponding detectors. [15, p. 93]

A typical choice for the light source is a tungsten halogen lamp. The monochromator is used to choose the measurement wavelength. Absorption spectrum is obtained by scanning over the desired wavelength range. Mirror M_5 is semi-transparent, and it splits the incident beam in two parts. One of the beams is directed to the sample while the other one goes through the reference channel. The signals from the sample and reference chambers, U_s and U_r , can now be measured simultaneously, and the ratio of the signals is written as $S(\lambda) = \frac{U_s}{U_r}$. The simultaneous detection of the sample and reference signals decreases the sensitivity to small fluctuations of light

source intensity, since both the reference channel and sample channel intensities change simultaneously, and the ratio does not change. [15, p. 92–94]

Ideally, the mirror splits the beam into two equal parts in the whole wavelength range, say, from 200 to 900 nm. In practice, however, there are always deviation from the 50 % transmittance at some part of the spectral range, and other components after M_5 cause further errors as well. The instrument effects are taken into account by measuring the *instrument response spectrum*, or *baseline*, with empty sample and reference compartments. Let us denote the baseline spectrum with $R(\lambda) = \frac{U_s^0(\lambda)}{U_r^0(\lambda)}$. Measuring the baseline spectrum increases the accuracy in the absorption spectrum measurement. [15, p. 92–94]

There are also other factors that affect the output signal. Many chromophores cannot be measured as is, but they have to be dissolved in some solvent. A liquid sample can only be measured in a cuvette. Then, the measured signal contains information on the desired sample absorption, but also on absorption of the solvent and cuvette walls, as well as on reflections from the cuvette walls. To obtain the spectrum of the sample only, a reference sample is used: a similar cuvette is filled with the same solvent and placed at the reference compartment. Now, let us denote the contributions from the sample, the cuvette and the solvent as transmittances: $T_s(\lambda)$ for the sample, $T_c(\lambda)$ for the absorption of the cuvette, $T_r(\lambda)$ for the reflections from the cuvette walls, and $T_{sol}(\lambda)$ for the solvent absorption. [15, pp. 92–95] Thus, the measured signal, or the ratio of the signals from the sample and reference channels is [15, p. 94]

$$S(\lambda) = \frac{U_s^0(\lambda)T_s(\lambda)T_c(\lambda)T_{sol}(\lambda)T_r(\lambda)}{U_r^0(\lambda)T_c(\lambda)T_{sol}(\lambda)T_r(\lambda)} = T_s(\lambda)\frac{U_s^0(\lambda)}{U_r^0(\lambda)} = T_s(\lambda)R(\lambda). \quad (3.2)$$

The transmittance spectrum for the sample only is calculated from Equation 3.2:

$$T_s(\lambda) = \frac{S(\lambda)}{R(\lambda)}, \quad (3.3)$$

and the absorbance spectrum

$$A_s(\lambda) = -\log T_s(\lambda). \quad (3.4)$$

Once the absorption spectrum is known, one can calculate for example the molar absorption coefficient from Equation 2.12, if the concentration of the sample solution is known.

In practical work, one can use the same baseline for several measurements. The baseline measurement needs to be repeated from time to time, depending on the long term stability of the particular instrument. [15, pp.102–103]

An important part of the measurement process are the cuvettes. Typical optical path lengths, or thicknesses of the cuvette, are 1 mm and 1 cm. Most common materials for the cuvettes are quartz and optical glass. Glass cuvettes can be used at wavelengths down to ca. 300 nm, and quartz cuvettes even at 200 nm. Usually, one uses two cuvettes of the same material with exactly the same optical path length, a *matching pair*. Matching pairs of cuvettes are designed to have identical absorption spectra when filled with the same solvent, and they provide a means for comparing the absorbances of different samples. In order to prevent scratches, many cuvettes are manufactured with two clear walls and two frosted walls. [15, pp. 100–103]

The instrument used in this work is a two-channel Shimadzu UV-3600 UV-VIS-NIR spectrophotometer. The measurable wavelength range is 185 – 3200 nm, and absorbances from -6 to 6 can be measured with 0.005 % accuracy.

Emission spectroscopy

Measuring an emission spectrum is as common task as measuring the absorption spectrum. Thus, the instruments need to be straightforward to use and the time required for the measurement needs to be rather short. [15, p. 107] Typically, fluorescence emission is measured, but from the viewpoint of the instrument there is no difference whether the emission is fluorescence or phosphorescence. An instrument measuring emission spectra is called a *spectrofluorometer* or a *fluorimeter*.

Formation of the measurable signal is more complicated in a spectrofluorometer than in a spectrophotometer, and absolute values of the emission intensities are usually not obtained. On the other hand, emission measurements are much more sensitive than in absorption spectroscopy, and therefore much lower sample concentrations can be studied than with absorption methods. [15, p. 107]

Figure 3.2 presents a schematic view of a spectrofluorometer. The first two parts, the light source and the monochromator, are similar to an absorption spectrophotometer, but the rest of the system is quite different. As shown in the figure, the sample is first excited with the light source at a chosen wavelength, the *excitation wavelength*, λ_{ex} . Different from the absorption spectrophotometer, the excitation light is not collected, and the measured light is produced by the sample. To be able to collect as many of the emitted photons as possible, the emission is collected at a right angle relative to the excitation light, and focused to the input of the detection system, as shown in Figure 3.2. Also the detector (usually a photomultiplier tube) is coupled with a monochromator to be able to monitor the intensity of the emitted light at different wavelengths. [15, pp. 107–110]

The measured signal, or the output voltage of the photomultiplier, U , depends on both the excitation wavelength, and the wavelength of the emitted photons (or the *emission wavelength*, λ_{em}). For the measurement of an emission spectrum, however,

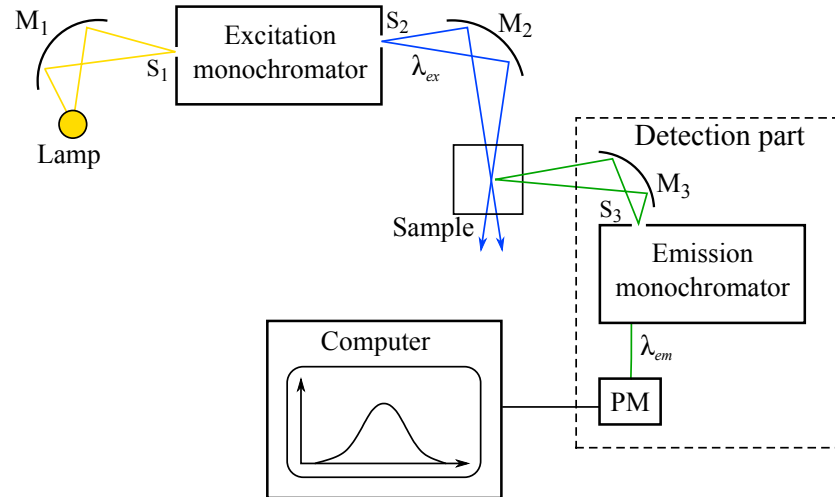


Figure 3.2. A schematic view of a spectrofluorometer. $M_1 - M_3$ are mirrors, $S_1 - S_3$ are the input and output slits of the monochromators, and PM is a photomultiplier tube. [15, p. 109]

the emission wavelength range is monitored with a fixed excitation wavelength, and the photomultiplier output voltage can be considered a function of the emission wavelength only: $U = U(\lambda_{em})$. It is also possible to monitor the emission at a fixed wavelength and scan different excitation wavelengths. Then, the measured spectrum is called an excitation spectrum, and the photomultiplier voltage can be expressed as $U = U(\lambda_{ex})$. [15, pp. 108–109]

Evaluation of the measured signal is somewhat more complicated in spectrofluorometers compared to spectrophotometers. Therefore, the factors affecting the measured signal are discussed only qualitatively.

The sample is emitting light in all possible directions, and collecting all emitted photons is practically impossible. Therefore, the measured signal will contain only a part of the emitted photons. Also, one has to take into account that only a narrow band of the emission spectrum can be measured at a time, so the concept of emission spectrum density should be used instead of intensity. In order to determine the total emission intensity, one must integrate the emission spectrum density over the measured wavelength range. There are also other things than the measured sample itself contributing to the emission intensity. A higher excitation intensity will yield higher emission intensities, so it is better to characterize the emission properties of the sample with the emission quantum yield and the shape of the emission spectrum instead of the emission intensity only. [15, pp. 111–114]

In addition to the previously discussed factors, the measured signal $U(\lambda)$ contains a contribution from sensitivity of the photodetector. Usually, commercial instruments contain a spectral correction function, S_c , provided by the manufacturer. With the correction, the emission spectrum of a sample is $U_c(\lambda) = U(\lambda)S_c(\lambda)$ [15,

pp. 111–114].

As mentioned earlier, the fluorescence quantum yield is an important quantity describing the fluorescent properties of a compound. Despite the fact that the fluorescence quantum yield does not depend on the excitation intensity, determining the absolute value of the quantum yield is often a very complicated task. Usually, the quantum yield is determined with a relative method instead of an absolute one: a reference compound with a known quantum yield, Φ_r , is used. The emission spectra of the measurable sample and the reference sample are then measured in identical conditions. Excitation wavelength is chosen so that the two samples have identical absorbance, and the monitoring range as well as monochromator slit widths are chosen equal. The corrected emission spectra for both samples are measured and the quantum yield is calculated from the integral intensities: [15, p. 114]

$$\Phi_F = \Phi_r \frac{\int_0^{\infty} U_c(\lambda) d\lambda}{\int_0^{\infty} U_{c,ref}(\lambda) d\lambda}, \quad (3.5)$$

where $U_c(\lambda)$ and $U_{c,ref}(\lambda)$ are the corrected spectra of the sample and the reference, respectively.

In this work, an ISA-Jobin Yvon-SPEX-Horiba Fluorolog-3-111 spectrofluorometer is used. The instrument has two detectors, **S** and **T**. The **S** detector can be used at wavelengths 290 – 850 nm, and **T** detector at 900 – 1700 nm. Only the **S** detector is used in this work. The **S** channel has a correction function to take into account the photodetector sensitivity. A correction function is also provided for channel **R**, the excitation spectrometer, at 240 – 600 nm to compensate for the sensitivity of the detector for the excitation intensity. The correction for the **R** channel is only used in measuring excitation spectra.

Similarly to the absorption measurements, most emission spectra are measured from a sample solution in a cuvette. The most typical cuvettes are made of glass or quartz, and have four clear walls (because of the right angle arrangement), 1 cm inner thickness and a square cross-section. Fluorescence cuvettes can be used in absorption spectrophotometers, if caution is taken when placing the cuvette into the sample holder to prevent any scratches. Scratches always induce additional reflections and unwanted scattering. [15, p. 122]

3.1.2 Time-resolved spectroscopy

In addition to steady-state measurements, time-resolved measurements are used to study the ESIPT reaction. Fluorescence lifetimes give information on the time scale of the reaction, and this information can only be achieved using time-resolved

measurement systems.

Time-Correlated Single Photon Counting (TCSPC)

The time-correlated single photon counting method (TCSPC) is a time-resolved emission method in the nanosecond and sub-nanosecond time domains. Since the fluorescence intensity is proportional to the population of the excited state, measuring the time profile of the emission provides a means for monitoring the reaction dynamics of photochemical reactions. [15, p. 151]

The TCSPC method is based on the fact that the probability of a photon reaching a detector after an excitation pulse after some time t is proportional to the fluorescence intensity at that time. [14, p. 173] Thus, with TCSPC one cannot obtain absolute values of the fluorescence intensity at different times, but only a time profile for the decay of the fluorescence intensity.

Figure 3.3 presents a schematic view of a TCSPC system. There are some properties somewhat similar to the steady-state emission spectrofluorimeters, namely the light source, the right angle position of the excitation and emission light beams, and the monochromator for the emitted light. In this work, a pulsed diode laser is used as the light source, but e.g. a flash lamp coupled with a monochromator can also be used [14, p. 173]. However, the mode-locked picosecond lasers give better time resolution and sensitivity, and provide a shorter data collecting time [15, p. 154].

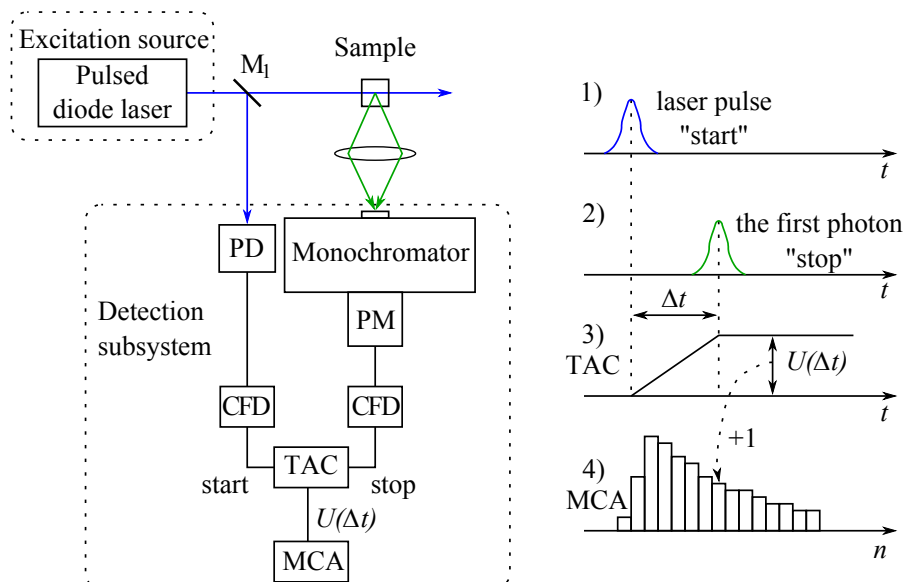


Figure 3.3. Scheme of the time-correlated single photon counting system. M_1 is a semi-transparent mirror, PD a photodetector, PM a photomultiplier tube, CFD a constant fraction discriminator, TAC a time-to-amplitude converter, and MCA a multichannel analyzer. [15, p. 152]

The principle of the TCSPC method is quite unique. The excitation beam is split

by the semi-transparent mirror M_1 . Part of the beam is directed to a photodiode (PD) and converted to an electric signal. A constant factor discriminator (CFD) ensures that timing of the signal at the CFD output does not depend on the amplitude of the input signal. The signal is further directed to a time-to-amplitude converter (TAC), which generates a voltage increasing linearly with time. [15, pp. 151–153; 17, pp. 104–105] Meanwhile, the rest of the pulse excites the sample. The emitted light is directed to a monochromator, which selects the desired monitoring wavelength (usually close to the wavelength of maximum emission determined by a steady-state measurement), and further to the photomultiplier tube (PM), which converts the detected photons to electric pulses. The electric signal is directed through a second CFD to the TAC, to stop the voltage increase. The generated voltage is then analyzed by a multichannel analyzer (MCA). The memory of the MCA is divided into different channels for different voltages, i.e. different time delays between the start and stop pulses. After each start–stop pulse sequence, the value of the channel corresponding to the correct voltage is increased by one. [14, pp. 173–175; 15, pp. 151–153] In other words, every time an emitted photon reaches the photomultiplier, the value of the MCA channel corresponding to the time delay of the photon is increased by one. A series of measurements results in an emission profile of the sample with discrete time steps. A large number of repeated measurements is needed, because not all photons generate a signal that reaches the MCA. [15, p. 153] The formation of the emission decay profile is depicted in Figure 3.3 on the right.

For a good data fitting, the temporal *instrument response*, or the shape and duration of the excitation pulse, has to be known. The instrument response is easily measured by tuning the monochromator to monitor the excitation wavelength, and directing the excitation light to the monochromator with a scattering sample, such as an aluminium plate. [15, p. 162]

The main parts of the TCSPC system used in this work include a PDL800-B pulsed diode laser driver, a fiber coupling unit (FCU) with a laser diode head, a PicoHarp 300 multichannel analyzer, all by PicoQuant, and a R3809U-50 photomultiplier tube (Hamamatsu). Emitting heads are available for four excitation wavelengths: 341 nm, 405 nm, 482 nm, and 660 nm. The time resolution of the system ranges from ≤ 100 ps to ca. 250 ps, depending on the excitation wavelength. The emission can be monitored in 300 – 850 nm range. Minimum length of a time channel in the MCA is 4 ps.

Fluorescence up-conversion

The time resolution of the TCSPC method is not good enough to study all the processes involved in the ESIPT reaction, especially the fluorescence of the locally excited state. This is why a shorter timescale method is needed. The timescale of the

studied enol relaxation is less than a picosecond, so optical methods in monitoring the emission are needed. The most widely used method for such measurements is the frequency up-conversion, or simply up-conversion (UC). [15, p. 217]

A schematic view of an up-conversion measurement system is presented in Figure 3.4. The light source is typically a Ti:sapphire laser coupled with a second-

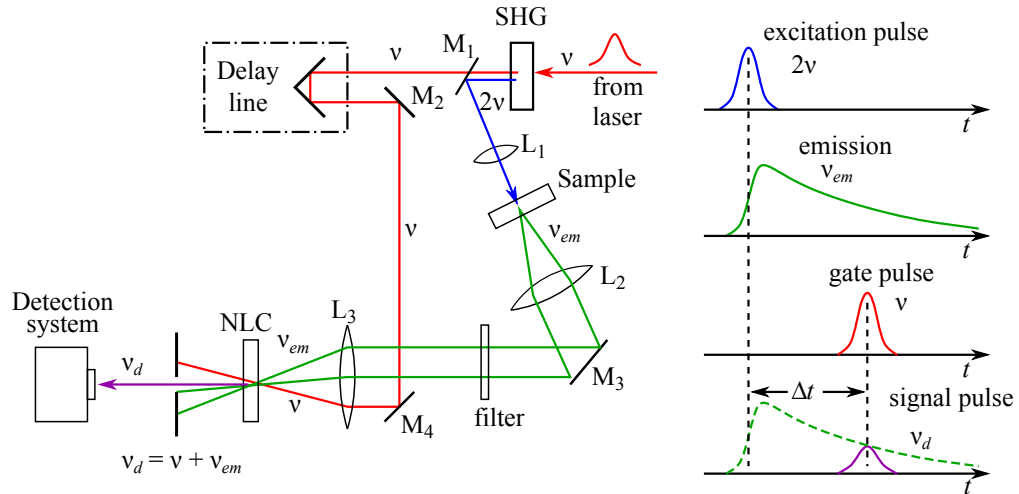


Figure 3.4. Scheme of the frequency up-conversion system. SHG is a second-harmonic generator, $M_1 - M_4$ mirrors, $L_1 - L_3$ lenses, and NLC a non-linear crystal. [15, p. 218]

harmonic generator (SHG). The second-harmonic generator is used to convert the wavelength of the laser emission (ca. 800 nm) to the region of sample absorption (ca. 400 nm). After the second-harmonic generation, there are two beams: the second-harmonic pulse and the fundamental pulse. As depicted in the figure, the second harmonic is directed to the sample via a dichroic mirror (M_1), and the fundamental, or the “gate” pulse is directed to a delay line. The emitted light from the sample and the gate pulse are both directed to the same non-linear crystal (NLC), which combines these two pulses, generating the measurable pulse. Before the NLC, the second harmonic pulse not absorbed by the sample is filtered out from the signal with a coloured filter. [15, pp. 217–218] The intensity of the measured signal is proportional to the product of the gate and sample emission intensities, and its frequency is the sum of the two frequencies; thus, the name frequency up-conversion [15, pp. 218–219]. Correspondingly, the wavelength of the up-converted signal, λ_d , is [15, p. 218]

$$\lambda_d = (\lambda_g^{-1} + \lambda_{em}^{-1})^{-1}, \quad (3.6)$$

where λ_g is the wavelength of the gate pulse and λ_{em} the emission wavelength.

Because the up-converted signal is generated only when the gate pulse and the emission pulse arrive simultaneously at the NLC, and because the gate pulse is usually much shorter in time than the emission pulse, the emission profile of the

sample can be measured by repeating the measurement with different gate pulse delays, as depicted on the right in Figure 3.4. The up-converted signal is detected by a photomultiplier coupled with a monochromator. [15, pp. 217; 39] The short time-resolution is achieved because the detection system itself can work in a steady-state mode [40, p. 210]. Thus, the frequency up-conversion method provides one of the few means for emission spectroscopy in the sub-picosecond time scale.

In order to obtain a good data fitting, the instrument response function is needed for up-conversion measurements as well. Unlike in the TCSPC measurements, measuring the instrument response experimentally is not a simple task. In the up-conversion scheme, the instrument response can be measured by passing the second harmonic to the NLC by removing the sample and the coloured filter, and tuning the detection monochromator to $\nu + 2\nu = 3\nu$. Carrying out the measurement is complicated: the pulses are short, so the delay line needs to be carefully adjusted to obtain a signal. Furthermore, the instrument response in a real measurement may be different because the time resolution of the pulse depends on wavelength. [15, pp. 223-224]

In the usual case, a simulated instrument response can be used instead of the experimentally determined response. The excitation pulse is assumed to be a Gaussian pulse, and the pulse width can be fitted together with the experimental data to obtain the simulated excitation pulse. The Gaussian pulse approximated instrument response gives usually sufficiently accurate results and a narrow pulse width (ca. 0.2 ps). [15, p. 225] Since the Gaussian approximation is easy to use and gives accurate fluorescence lifetimes, it is used as the simulated instrument response in this work.

3.2 Materials

The 10-hydroxybenzo[*h*]quinoline derivatives used in this Thesis were synthesized in the Institute of Organic Chemistry at the Polish Academy of Sciences by Dr. Daniel T. Gryko and co-workers.

Structures of the compounds used in this work are shown in Figure 3.5. The compounds can be divided into several groups according to the substituents. There are five compounds substituted at position 4, arranged in Figure 3.5 according to the electron donating ability of the substituent. The morpholine and methyl substituents are expected to act as electron donors, whereas the cyano and tosyl groups as well as the (trifluoromethyl)styryl substituent are electron-withdrawing. This group is the most interesting regarding this Thesis, because the effect of different substituents at the same position can be studied, testing the hypothesis formulated by Chou *et al.* (see Section 2.3.4). The second group are the 6- and 7-nitro-substituted compounds. As discussed in Section 2.3.4, different behaviour is expected in the ESIPT

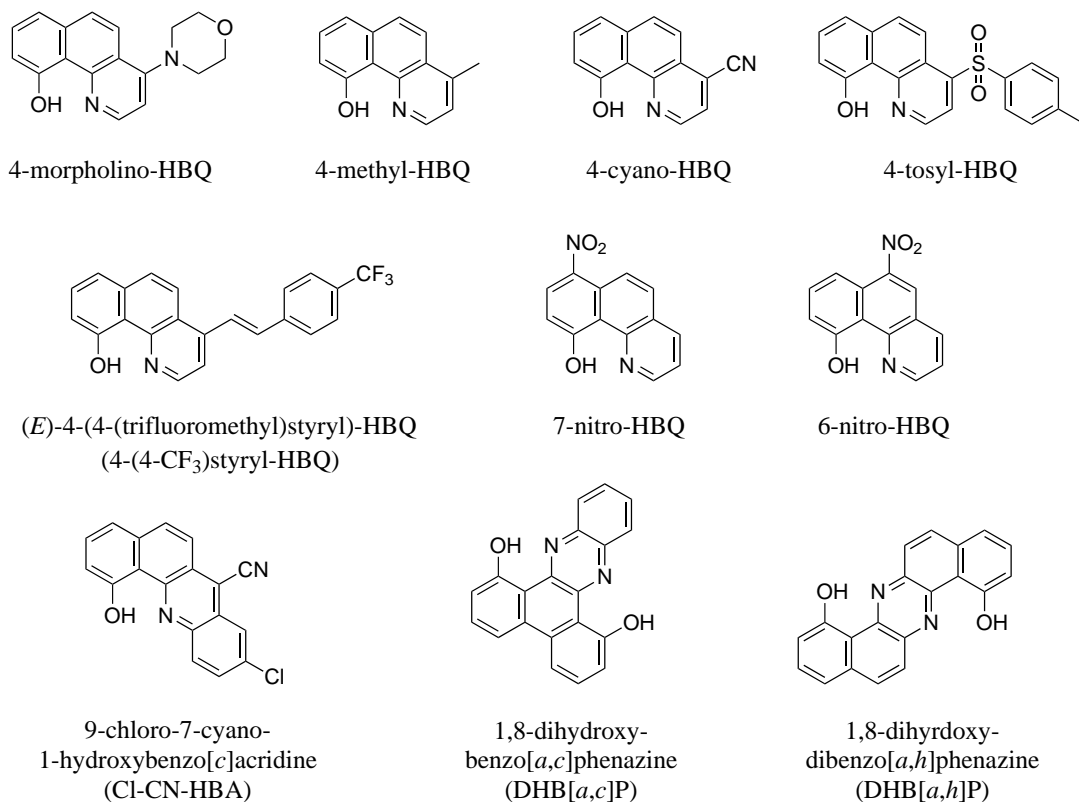


Figure 3.5. Structures of the compounds used.

rate of these two compounds because of the different location of the substituent in the molecule. In 9-chloro-7-cyano-1-hydroxybenzo[*c*]acridine (Cl-CN-HBA), the conjugation is extended further with the additional phenyl group. The last two compounds, DHB[*a,c*]P and DHB[*a,h*]P, form a special group of compounds with two sites for the proton transfer.

The compounds were studied in solutions. Different solvents and washing agents were used: dichloromethane (DCM), toluene, and chloroform were purchased from Sigma-Aldrich, and tetrahydrofuran (THF) and acetonitrile (MeCN) from VWR International. All these solvents were of HPLC grade. Ethanol (≥ 96.1 vol-%) was purchased from Altia. All solvents were used as purchased.

In addition to the compounds synthesized by Dr. Gryko and co-workers, a fluorescent dye Rhodamine 6G (purchased from Arcos Organics) was used. All solid compounds were used without further purification.

3.3 Experimental

All studies were carried out in solution. Three solvents with different polarities were used: polar acetonitrile, moderately polar tetrahydrofuran, and non-polar toluene. Steady-state and TCSPC measurements were carried out in 1 cm cuvettes, so the

solutions were dilute (ca. 10^{-5} M). The up-conversion measurement requires a special cuvette with ca. 1 mm optical path length, so more concentrated solutions (ca. 10^{-3} M) were prepared.

3.3.1 Absorption and emission spectra

For the steady-state emission measurements, the desired sample absorbance at the excitation wavelength is $A \approx 0.2$. A natural choice for the excitation wavelength is near the absorption maximum. Therefore, the samples were prepared to achieve the desired absorbance at the maximum.

The molar absorption coefficients at the first absorption maximum for the compounds were provided by Dr. Gryko’s group, and they are presented in Table 3.1. Given the desired absorbance and the molar absorption coefficient, the desired sample concentrations can be calculated. The target concentrations are also shown in Table 3.1.

Because solutions with micromolar concentration are difficult to prepare directly from solid compounds, stock solutions with millimolar concentrations were first prepared. Approximately 0.5 – 1 mg of each compound was dissolved in 0.5 – 1 mL dichloromethane. The concentrations of the stock solutions were not accurate, because the mass could not be determined accurately. However, since the important quantity is the absorbance and not the concentration, the inaccurate stock solutions could be used.

Table 3.1. Molar absorption coefficients of the compounds at first absorption maximum, position of the maximum in terms of wavelength, and desired sample concentrations with $A = 0.2$ at the maximum.

Compound	λ_{abs} (nm)	ϵ ($M^{-1} \text{ cm}^{-1}$)	c (μM)
4-morpholino-HBQ	373	8,700	23.0
4-methyl-HBQ	372	9,800	20.4
4-cyano-HBQ	408	8,200	24.4
4-tosyl-HBQ	402	6,300	31.7
4-(CF ₃)styryl-HBQ	394	7,500	26.7
7-nitro-HBQ	371	12,500	16.0
6-nitro-HBQ	339	7,700	26.0
Cl-CN-HBA	461	10,200	19.6
DHB[<i>a,c</i>]P	428	17,900	11.2
DHB[<i>a,h</i>]P	484	8,700	23.0

To prepare the sample solutions for absorption and emission measurements, the stock solutions were diluted 100 times by pipetting 40 μL stock solution to a clean test tube, evaporating the dichloromethane and adding 4 mL of the desired solvent (MeCN, THF or toluene). The absorption spectra were measured, and the concentration of each solution was changed to achieve the target absorbance either by

adding solvent or by pipetting more stock solution to a clean test tube, evaporating DCM, and adding the sample solution on top of the solid compound.

Absorption spectra for the sample solutions in MeCN, THF and toluene were measured in the 200 – 850 nm range. Each measurement was conducted in a matching pair of quartz cuvettes, placing the sample solution in one cuvette and pure solvent in the other. Before and after each measurement, the cuvettes were washed with chloroform. If necessary, also ethanol and deionized water were used for washing. Using pure solvent in the reference channel enables monitoring of the sample absorbance without contribution of the solvent. At short wavelengths, however, the solvent absorbance is so high that sample absorbance cannot be determined accurately. For example, toluene absorbs at wavelengths shorter than ca. 280 nm. Thus, in toluene, no information about the absorbing efficiency of the compounds was obtained below 280 nm.

Emission spectra for the compounds were measured in glass fluorescence cuvettes with 1 cm optical length and a square cross section. The cuvettes were washed similarly as the absorption cuvettes. The measurement parameters were kept identical for each compound in different solvents to be able to directly compare the emission intensities in different solvents. Excitation wavelength was chosen near the first absorption maximum, so that the excitation would be as similar as possible for the compound in different solvents. Emission was monitored at wavelengths starting from 10 nm longer than the excitation wavelength. The slit widths of both monochromators (see Section 3.1.1) were chosen quite large to obtain a sufficient signal-to-noise ratio. If necessary, the second-order diffraction of the excitation light was filtered out from the signal by using a coloured filter. All spectra were collected in 1 nm wavelength steps, and with 0.5 s acquisition time at each wavelength. The used excitation wavelengths, monitoring ranges and used monochromator slits for each compound, as well as the choice of filter are presented in Table 3.2.

Table 3.2. Measurement conditions for the emission spectra of the compounds.

Compound	λ_{ex} (nm)	Monitoring (nm)	Slit width (nm)	Filter
4-morpholino-HBQ	370	383 – 800	4	Yellow 12
4-methyl-HBQ	374	384 – 800	4	Yellow 12
4-cyano-HBQ	409	419 – 800	5	—
4-tosyl-HBQ	402	412 – 790	5	—
4-(CF ₃)styryl-HBQ	363	373 – 700	5	—
7-nitro-HBQ	370	380 – 800	4	Yellow 12
6-nitro-HBQ	328	338 – 850	5	Colourless 8
Cl-CN-HBA	461	471 – 850	5	—
DHB[<i>a,c</i>]P	429	439 – 830	5	—
DHB[<i>a,h</i>]P	484	494 – 850	5	—

The transmittance spectra of the used filters are presented in Appendix 1. The spectra show that no excitation light is transmitted to the emission monochromator with a filter, thus removing the second-order scattering from the signal.

3.3.2 Fluorescence quantum yields

Fluorescence quantum yields for the compounds were determined by the relative method described in Section 3.1.1. For 4-morpholino-HBQ, 4-methyl-HBQ and 7-nitro-HBQ in THF, Rhodamine 6G was used as a reference compound. Once the fluorescence quantum yields for these compounds in one solvent were known, one of them was chosen as the reference compound for all other compounds. Any of the three compounds could have been used, since they all showed a moderate fluorescence quantum yield, so that the emission spectrum of the reference compound and the studied sample can be measured with the same measurement parameters, being still able to distinguish the sample signal from noise. However, 4-morpholino-HBQ was chosen, because its emission intensity did not depend on the choice of solvent, and there was a sufficient amount of the compound to be used. All fluorescence quantum yield measurements were carried out in the same glass fluorescence cuvettes as the emission spectrum measurements.

First, a stock solution of Rhodamine 6G solution was prepared by dissolving ca. 1.5 mg of the solid compound in 1.5 mL ethanol. Then, the measurable solution was prepared by diluting the stock solution by ca. 60 times: 70 μL of the stock solution was diluted to 4 mL. Sample solutions for the compounds under study were prepared in THF. The stock solutions described previously were diluted by ca. 100 times, similarly to the emission measurements.

To determine the excitation wavelength for each sample–reference pair, the absorption spectra for both the reference solution and the samples were measured in the 200 – 850 nm range, similarly as described previously. An intersection of the sample and reference absorption spectra with $A \approx 0.2$ was chosen as the excitation wavelength for each sample–reference pair. Therefore, the excitation wavelength for each pair was $\lambda_{ex} \approx 350$ nm. The exact excitation wavelengths as well as the monitoring wavelengths are presented in Table 3.3. Slit widths for the excitation

Table 3.3. Measurement conditions for the fluorescence quantum yields for 4-morpholino-HBQ, 4-methyl-HBQ, and 7-nitro-HBQ using Rhodamine 6G as a reference compound.

Compound	λ_{ex} (nm)	Monitoring (nm)
4-morpholino-HBQ	356	366 – 850
4-methyl-HBQ	354	364 – 850
7-nitro-HBQ	353	363 – 850

and emission monochromators were 2 and 1 nm, respectively. Measurements were carried out in 1 nm wavelength steps with 0.5 s acquisition time at each wavelength, and the second-order diffraction of the excitation light was filtered out with the yellow filter 10. Transmittance spectrum of the filter is shown in Appendix 1.

Fluorescence quantum yields for the rest of the compounds in THF were estimated using 4-morpholino-HBQ as a reference compound. Again, the stock solutions were diluted ca. 100 times to achieve an absorbance near 0.2. Absorption spectra for all compounds were measured similarly as described above, and an intersection of the sample and reference absorption spectra with $A \approx 0.2$ was chosen as the excitation wavelength for each sample–reference pair. If necessary, concentration of the sample solutions were changed by evaporating some solvent to obtain an intersection with a suitable absorbance. The chosen excitation wavelengths as well as the monitoring wavelengths ranges are presented in Table 3.4. Both monochromator slits were 5 nm

Table 3.4. Measurement conditions for the fluorescence quantum yields for the compounds in THF using 4-morpholino-HBQ as a reference compound.

Compound	λ_{ex} (nm)	Monitoring (nm)	Filter
4-methyl-HBQ	380.2	390 – 850	Yellow 11
4-cyano-HBQ	308.5	318 – 850	Colourless 300
4-tosyl-HBQ	314	324 – 850	WG360
4-(CF ₃)styryl-HBQ	364	374 – 850	Yellow 10
7-nitro-HBQ	340	350 – 850	Yellow 12
6-nitro-HBQ	382	392 – 850	Yellow 11
Cl-CN-HBA	317	327 – 850	WG360
DHB[<i>a,c</i>]P	317.5	327 – 850	WG360
DHB[<i>a,h</i>]P	316	326 – 850	WG360

in all measurements, and all spectra were collected with 1 nm wavelength steps and a 0.5 s acquisition time at each wavelength. If necessary, the second-order diffraction of the excitation light was filtered out. The chosen filters for each sample–reference pair are also shown in Table 3.4, and the transmittance spectra of the filters are presented in Appendix 1. As shown in the table, 4-methyl-HBQ and 7-nitro-HBQ were measured using 4-morpholino-HBQ as a reference compound as well, to be able to compare the quantum yields obtained with two different references.

Fluorescence quantum yields for each compound in MeCN and toluene were estimated using the same compound in THF as reference. Since the emission spectra were measured with identical measurement conditions in all solvents, the obtained fluorescence quantum yield in THF could be used as a reference quantum yield in other solvents. Thus, fluorescence quantum yields in MeCN and toluene were calculated with Equation 3.5 using the quantum yield in THF and the measured emission intensities.

3.3.3 Time-resolved measurements

Sample solutions for the up-conversion measurements were prepared directly from solid compounds. Because the cuvette for these measurements has a thickness of ca. 1 mm, higher absorbance is needed ($A \approx 1.0$ at the excitation wavelength). Therefore, the desired concentrations are $c \approx 1$ mM. The samples were prepared by dissolving ca. 1 – 2 mg of the compound into 1 – 2 mL of the desired solvent. Absorption spectrum of each sample was measured in 300 – 850 nm range in 1 mm glass cuvettes, using pure solvent as a reference. If necessary, more solvent was added to achieve the target absorbance.

After the desired sample concentration was obtained, the sample was moved into the round cuvette. The possible sample degradation during the up-conversion measurements was monitored by measuring absorption spectra of each sample in the round cuvette before and after each up-conversion measurement.

The up-conversion measurement could only be carried out for six of the compounds. The emission of Cl-CN-HBA and DHB[*a,h*]P is shifted so much to the red, that it cannot be monitored with the used instrument. For 4-(CF₃)styryl-HBQ, the situation is the opposite: the emission is at too short wavelengths to be monitored. The absorption spectra of 6-nitro-HBQ showed major dependence on the solvent, so selecting one excitation wavelength would have been difficult.

The TCSPC measurements were carried out for the same compounds than the up-conversion measurements. For TCSPC measurements, sample solutions similar to the absorption and emission measurements were used. The measurements were carried out in the same fluorescence cuvettes as the steady-state emission measurements.

The choices of excitation and monitoring wavelengths require knowledge on the absorption spectra of the compounds. Thus, selection of the excitation and monitoring wavelengths in the time-resolved measurements is explained in Section 4.2.

4 RESULTS AND DISCUSSION

This Chapter exhibits the results of this study. Results from both steady-state and time-resolved measurements are presented and shortly discussed. Absorption and emission spectra of the compounds are shown, and both substituent and solvent effects are demonstrated. In the time-resolved section, fluorescence lifetimes of the compounds are evaluated, both in picosecond and nanosecond time scales. Reasons for the different behaviour of different compounds are discussed.

4.1 Steady-state measurements

Absorption and emission maxima as well as the corresponding Stokes shifts for the compounds are presented in Table 4.1. As can be seen from the table, the Stokes shifts are indeed enormous for most of the compounds, ranging from ca. 200 nm to as large as 320 nm. The Stokes shifts are somewhat similar to the value reported for the non-substituted HBQ, ca. 250 nm [9].

Table 4.1. Wavelengths of the absorption and emission maxima for the compounds and the Stokes shifts.

Compound	λ_{abs} (nm)	λ_{em} (nm)	Stokes shift (nm)	Compound	λ_{abs} (nm)	λ_{em} (nm)	Stokes shift (nm)
4-morpholino-HBQ				7-nitro-HBQ			
MeCN	370	596	226	MeCN	368	566	198
THF	373	602	229	THF	370	573	203
Toluene	376	604	228	Toluene	370	577	207
4-methyl-HBQ				6-nitro-HBQ			
MeCN	370	604	234	MeCN	329	582	253
THF	374	608	234	THF	377	585	208
Toluene	376	609	233	Toluene	342	587	245
4-cyano-HBQ				Cl-CN-HBA			
MeCN	402	724	310	MeCN	458	740	282
THF	408	722	311	THF	461	746	285
Toluene	411	724	306	Toluene	464	745	281
4-tosyl-HBQ				DHB[<i>a,c</i>]P			
MeCN	396	716	320	MeCN	423	724	301
THF	402	715	313	THF	432	722	290
Toluene	406	714	308	Toluene	429	724	295
4-(CF ₃)styryl-HBQ				DHB[<i>a,h</i>]P			
MeCN	390	470	80	MeCN	477	743	266
THF	396	456	60	THF	485	756	271
Toluene	399	447	48	Toluene	488	754	266

Absorption and emission spectra for the compounds are presented as figures in Appendix 2. The presented emission spectra are the corrected spectra (see Section 3.1.1), and the contribution of the coloured filters is cancelled by dividing the emission intensity by the filter transmittance at each wavelength.

A slight hypsochromic effect with increasing solvent polarity was observed for most of the compounds in both absorption and emission spectra. That is, the absorption and emission maxima are located at shorter wavelengths in the more polar solvents because of the change in solvent–solute interactions [14, pp. 200–202]. However, this effect is not significant. For most of the compounds, the change in the position of the maximum emission is smaller than the slit width of the emission monochromator, which in this case is 5 nm. Thus, the inaccuracy in determining the maximum emission wavelength is greater than the differences between the maxima in different solvents.

The only compounds with a clear solvent effect in the position of absorption and emission maxima are 6-nitro-HBQ and 4-(CF₃)styryl-HBQ. The absorption spectra of 6-nitro-HBQ has quite different shape than all the other compounds. There is a clear absorption maximum only in the least polar solvent, toluene. Moreover, the absorption maximum is located at a wavelength much shorter than for any of the other compounds. In tetrahydrofuran and acetonitrile, the absorption coefficient is increased at shorter wavelengths, with no clear absorption maximum. The reason for the unexpected behaviour is not clear. The nitro substituent at the cyclohexa-2,4-dienone part of the molecule might affect the energies of the HOMO and LUMO levels of the compound and cause the different behaviour in the absorption spectra in different solvents.

The emission spectrum of 4-(CF₃)styryl-HBQ shows remarkable differences in the positions of the emission maxima in different solvent polarities. In fact, it seems that the main component contributing to the emission spectrum is the enol emission, not the expected keto emission. The reason might be the extremely electron-withdrawing nature of the substituent, which leads to stabilization of the enol tautomer and emission at shorter wavelengths.

4.1.1 Fluorescence quantum yields

Fluorescence quantum yields for 4-morpholine-HBQ, 4-methyl-HBQ and 7-nitro-HBQ in THF were calculated from Equation 3.5 using Rhodamine 6G as the reference compound. Fluorescence quantum yield for Rhodamine 6G was taken 0.95 [40]. Table 4.2 shows the positions of the emission maxima for each sample and the corresponding reference measurement, as well as the estimated quantum yields for the compounds.

Table 4.2. Maximum emission wavelengths and the fluorescence quantum yields for 4-morpholino-HBQ, 4-methyl-HBQ, and 7-nitro-HBQ using Rhodamine 6G as a reference.

Compound	$\lambda_{em,s}$ (nm)	$\lambda_{em,ref}$ (nm)	Φ_s	Φ_s (%)
4-morpholino-HBQ	603	560	0.0210	2.10
4-methyl-HBQ	606	559	0.0138	1.38
7-nitro-HBQ	574	559	0.0212	2.12

Fluorescence quantum yields for the other compounds in THF were estimated using 4-morpholino-HBQ as a reference compound. The estimated fluorescence quantum yields in THF could be used as reference quantum yields in MeCN and toluene for each compound. The estimated fluorescence quantum yields for the compounds in all studied solvents are presented in Table 4.3.

Table 4.3. Fluorescence quantum yields for the compounds in THF using 4-morpholino-HBQ in THF as a reference, and fluorescence quantum yields in MeCN and toluene using the quantum yields in THF as references.

Compound	MeCN		THF		Toluene	
	Φ_s	Φ_s (%)	Φ_s	Φ_s (%)	Φ_s	Φ_s (%)
4-morpholino-HBQ	0.0223	2.23	0.0210	2.10	0.01960	1.96
4-methyl-HBQ	0.0143	1.43	0.0140	1.40	0.01375	1.38
4-cyano-HBQ	0.0006	0.06	0.0005	0.05	0.00063	0.06
4-tosyl-HBQ	0.0006	0.06	0.0007	0.07	0.00077	0.08
4-(CF ₃)styryl-HBQ	0.0019	0.19	0.0024	0.24	0.00213	0.21
7-nitro-HBQ	0.0016	0.16	0.0236	2.36	0.03051	3.05
6-nitro-HBQ	0.0005	0.05	0.0020	0.20	0.00132	0.13
Cl-CN-HBA	0.0008	0.08	0.0006	0.06	0.00075	0.08
DHB[<i>a,c</i>]P	0.0001	0.01	0.0001	0.01	0.00015	0.02
DHB[<i>a,h</i>]P	0.0003	0.03	0.0003	0.03	0.00029	0.03

As can be seen from Table 4.3, fluorescence quantum yields for most of the compounds are low. The three compounds measured with the Rhodamine 6G reference are the only ones with a quantum yield higher than 1 %. Fluorescence quantum yields for 4-methyl-HBQ and 7-nitro-HBQ in THF were estimated with the 4-morpholino-HBQ reference as well to be able to compare the results obtained with the different references. For both compounds, the fluorescence quantum yields in THF determined with the different reference compounds are quite similar: for 4-methyl-HBQ, $\Phi_F = 1.38$ % with Rhodamine 6G, and $\Phi_F = 1.40$ % with 4-morpholino-HBQ as the reference, and for 7-nitro-HBQ, $\Phi_F = 2.12$ % with Rhodamine 6G, and $\Phi_F = 2.36$ % with 4-morpholino-HBQ as the reference, respectively. Thus, it can be concluded that using 4-morpholino-HBQ as the reference compound, the fluorescence quantum yields for the compounds can be trusted at least as a maximum estimate.

4.1.2 Substituent effects

Figure 4.1 presents the absorption and emission spectra in toluene for four differently substituted compounds at position 4: 4-morpholino-HBQ, 4-methyl-HBQ, 4-cyano-HBQ, and 4-tosyl-HBQ. The results meet the expectations formulated in

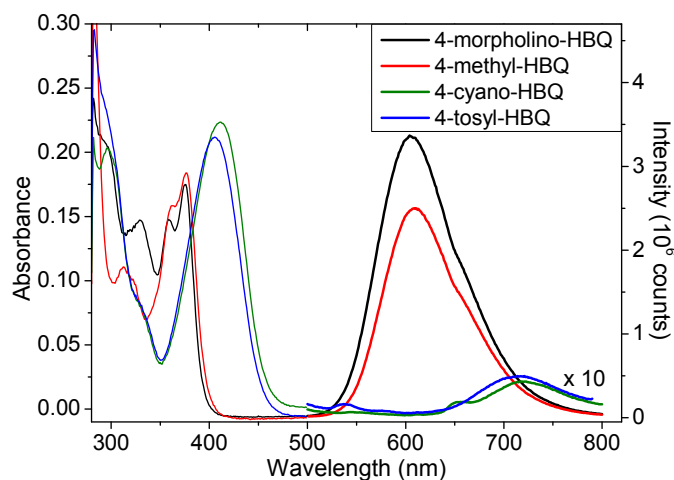


Figure 4.1. Absorption and emission spectra in toluene for 4-morpholino-HBQ, 4-methyl-HBQ, 4-cyano-HBQ, and 4-tosyl-HBQ. Absorption spectra are presented with solid lines, and emission spectra with heavy solid lines. Emission spectra of 4-cyano-HBQ and 4-tosyl-HBQ are multiplied by 10.

Section 2.3.4 quite well. There is a small but surprisingly clear change in the absorption spectra when going from the electron-donating substituents to the electron-withdrawing substituents. The absorption is shifted to longer wavelengths, which can be noticed in the figure, but also in Table 4.1 as well: the absorption maximum is located at 376 nm for the compounds substituted with electron-donating group, whereas for 4-tosyl-HBQ and 4-cyano-HBQ it is shifted to 406 and 411 nm, respectively. Moreover, the fine structure of the maximum absorption band is lost in the compounds substituted with electron-withdrawing groups. Unlike expected in Section 2.3.4, a substituent effect is visible in the absorption spectra, albeit rather small. The shift of the absorption maximum to longer wavelengths with electron-withdrawing substituents suggests a decrease in the HOMO–LUMO energy gap of the enol tautomer compared to non-substituted HBQ (absorption maximum at 377 nm in benzene [9]). On the other hand, comparing the absorption maxima of 4-morpholino-HBQ and 4-methyl-HBQ to the non-substituted compound suggests that substituting the HBQ core with an electron-donating group, the HOMO–LUMO energy gap is practically not affected.

In the emission spectra, the substituent effect is much more dramatic, as expected. The emission is clearly shifted to longer wavelengths when going from the electron-donating morpholine and methyl substituents to the electron-withdrawing cyano

and tosyl groups. The observed result is in good agreement with the suggested change in HOMO–LUMO energy gap of the keto tautomer. With the electron-donating substituents, the emission maximum is shifted to shorter wavelengths, which corresponds to an increase in the HOMO–LUMO gap: 604 and 609 nm for 4-morpholino-HBQ and 4-methyl-HBQ, compared to 630 nm for the non-substituted HBQ (in benzene) [9]. Correspondingly, substituting the HBQ core with electron-withdrawing substituents, the HOMO–LUMO gap is decreased and the emission is shifted to longer wavelengths: the emission maxima are located at 714 and 724 nm for 4-tosyl-HBQ and 4-cyano-HBQ, respectively. Similarly to the absorption spectra, the electron-withdrawing substituents have a greater effect on the position of the emission maximum than the electron-donating ones.

Moreover, the emission intensity is drastically decreased for the compounds with an electron-withdrawing substituent. To be able to distinguish the signal from noise in Figure 4.1, a tenfold magnification of the spectra is needed. The reason for the decrease in the emission intensity is the increased reaction rate, which will be further discussed in Section 4.2.2.

Despite the fact that the absorption and emission spectra for non-substituted HBQ were measured in different solvent than the compounds studied here, the positions of the absorption and emission maxima can be quite safely compared. Benzene and toluene have almost the same polarity [41], and thus they are expected to interact with the solute similarly.

Out of the studied compounds, 4-methyl-HBQ is probably structurally closest to the non-substituted compound. Thus, quite similar emission properties are expected. However, the fluorescence quantum yields for the two compounds are quite different. According to Chou *et al.* [9], fluorescence quantum yield for the HBQ keto tautomer (in benzene solution) is 0.0025, or 0.25 %, ten times lower than that measured for 4-methyl-HBQ, and actually closer to the quantum yields determined for compounds with electron-withdrawing substituents. This is surprising, because the position of the emission maxima suggest similarity between the non-substituted HBQ and the compounds with electron-donating substituents.

4.1.3 Solvent effects

As discussed in Section 2.3.5, the change in the rate of the ESIPT process in different solvents is determined by the relative magnitude of the dipole moments of the enol and keto tautomers, and the following stabilization of one of the tautomers by the solvent. The change in the reaction rate can be observed, at least to some extent, in the steady-state emission spectra as well. If the excited state of a fluorescent species relaxes fast, the steady-state emission intensity is decreased.

For most of the compounds, no significant solvent effect is observed in the emission

spectra. The emission spectra in Appendix 2 show quite similar shape in different solvents. Also the fluorescence quantum yields for each compound (see Table 4.3) are quite similar in different solvents. Apparently, the intramolecular hydrogen bond is so strong that solvent interference on it is minimal, even in polar solvents. Based on this result, the concerted mechanism is tentatively proposed as the reaction mechanism of the ES IPT process in these compounds: a simultaneous proton and electron transfer in the structure, shielded from the solvent effect by the strong intramolecular hydrogen bond.

The nitro-substituted compounds show much greater solvent effect than the other compounds. The emission intensity and fluorescence quantum yield decrease drastically with the solvent polarity increase from the non-polar toluene to the moderately polar tetrahydrofuran and to the polar acetonitrile. Figure 4.2 presents the absorption and emission spectra for 7-nitro-HBQ and 6-nitro-HBQ.

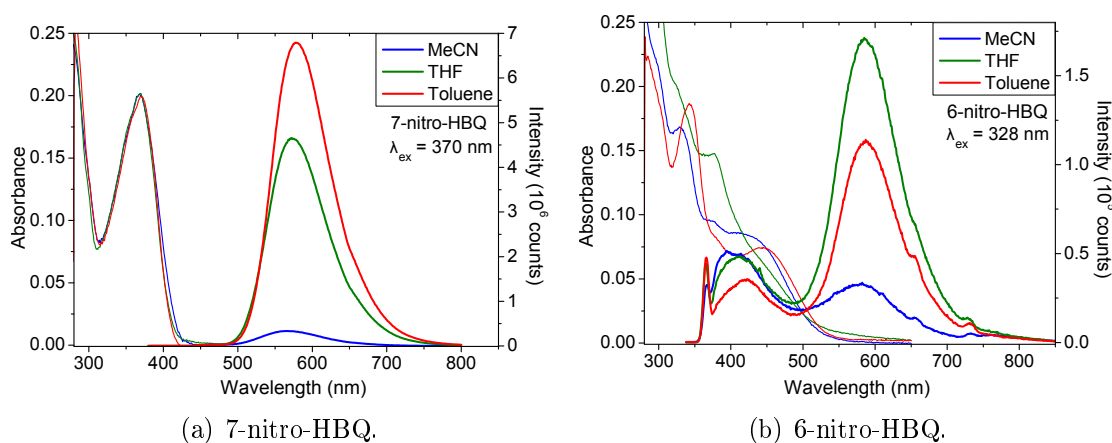


Figure 4.2. Absorption and emission spectra for the nitro-substituted HBQ derivatives in acetonitrile, tetrahydrofuran and toluene. Absorption spectra are presented with solid lines, and emission spectra with heavy solid lines.

As already discussed, increasing solvent polarity induces a small hypsochromic effect in the position of the emission maxima. However, this effect is minor compared to the effect of the solvent on the emission intensity. In THF, the fluorescence quantum yield of 7-nitro-HBQ is reduced to ca. 75 % of that in toluene. In acetonitrile, the difference is even greater: the fluorescence quantum yield in MeCN is reduced to ca. 5 % of that in toluene. Since the emission intensity and the reaction rate are inversely proportional, the reduction in keto tautomer emission intensity corresponds to a 1.3-fold increase in the rate of the relaxation of the keto tautomer in tetrahydrofuran compared to toluene. Respectively, the relaxation rate is ca. 20 times higher in acetonitrile than in toluene.

The fluorescence quantum yield of 6-nitro-HBQ in MeCN is ca. 40 % of that in toluene, which corresponds to a 2.6-fold increase in the keto tautomer relaxation rate.

Surprisingly, the fluorescence quantum yield in THF seems higher than in toluene: $\Phi_F = 0.20$ % in THF vs. $\Phi_F = 0.13$ % in toluene. The fluorescence quantum yields are so small that the difference can be explained by the inaccuracy in the fluorescence quantum yield measurement. Therefore, the only apparent conclusion is that there is a tendency of increased keto tautomer relaxation rate with increasing solvent polarity.

The increase in the relaxation rate with increasing solvent polarity suggests that the intramolecular hydrogen bond is for some reason more vulnerable to solvent perturbation in the nitro-substituted compounds than in other compounds. Perhaps the substitution of a nitro group at position 6 or 7 affects the energies of the HOMO and LUMO levels of the keto tautomer differently than substituting at position 4, causing weakening of the intramolecular hydrogen bond. A weaker hydrogen bond is then exposed to solvent perturbation, especially in the more polar solvents. If the solvent effect is caused by solvent perturbation on the intramolecular hydrogen bond, a corresponding increase in the enol emission is expected. However, in 7-nitro-HBQ this effect is not observed. In 6-nitro-HBQ, there is an increase in emission efficiency with increasing solvent polarity at ca. 370 – 470 nm, which could be enol emission. However, based on the discussion in Section 2.3.5, the ES IPT reaction seems to proceed via the proton-coupled electron-transfer mechanism or the concerted mechanism in the nitro-substituted compounds as well.

4.2 Time-resolved measurements

The up-conversion measurements were carried out in two sample series: 4-morpholino-HBQ, 4-methyl-HBQ and 7-nitro-HBQ, with $\lambda_{ex} = 390$ nm, and 4-cyano-HBQ, 4-tosyl-HBQ, and DHB[*a,c*]P, with $\lambda_{ex} = 410$ nm. Hereafter, the series are referred to as series 1 and series 2, respectively. As can be seen from Table 4.1, the compounds in series 1 have their absorption maxima at even shorter wavelengths, but because a Ti:sapphire laser was used as the fundamental light source, it could only be tuned to give 390 nm as the second harmonic wavelength.

Monitoring wavelengths were chosen according to the steady-state emission spectra (shown in Appendix 2). Since the excited-state lifetimes of both the enol and keto tautomers were searched for, three emission wavelengths were chosen: near the expected enol emission maximum, near the (keto) emission maximum, and on the longer-wavelength side of the emission spectrum. Therefore, monitoring wavelengths were 500, 600 and 660 nm for series 1, and 610, 710 and 750 nm for series 2. Total time window for the up-conversion measurements was ca. 250 ps for series 1, and ca. 100 ps for series 2, respectively.

The TCSPC measurements were carried out to determine the lifetime of the keto tautomer excited state more accurately. Therefore, the measurements were carried

out for only those compounds that were studied by the up-conversion method. Because the TCSPC system uses laser diodes as a light source, the choice of excitation wavelength was limited to 405 nm for all samples. Emission was monitored near the (keto) emission maximum, i.e. at 600 nm for series 1, and at 710 nm for series 2. Total time windows for the measurements were 20 and 15 ns for series 1 and 2, respectively.

Multi-exponential fitting functions were used to estimate the fluorescence lifetimes. For up-conversion measurements, the best fit was obtained with three exponents. A *global fitting* was used, i.e. all three emission decay curves measured for each sample in one solvent were fitted simultaneously to obtain common fluorescence lifetimes regardless of the monitoring wavelength. For TCSPC measurements, a bi-exponential fitting function was used. Since the TCSPC measurements were carried out at one monitoring wavelength only, no global fitting was needed.

It was observed that the two sample series behave quite differently, so the results are discussed in separate Sections for each sample series.

4.2.1 4-morpholino-HBQ, 4-methyl-HBQ, and 7-nitro-HBQ

Figure 4.3 presents the fluorescence emission decay curve obtained from the up-conversion measurement for 4-morpholino-HBQ in toluene. Figure 4.3(a) presents the total measured time window (from 0 to ca. 300 ps), and Figure 4.3(b) presents the same data in the expended time window at the beginning of the decay (from 0 to 10 ps). The symbols denote the measured data points, and the solid lines show the fitting function. Similar fluorescence emission decay curves for all compounds in this sample series in all studied solvents can be found in Appendices 3 – 5.

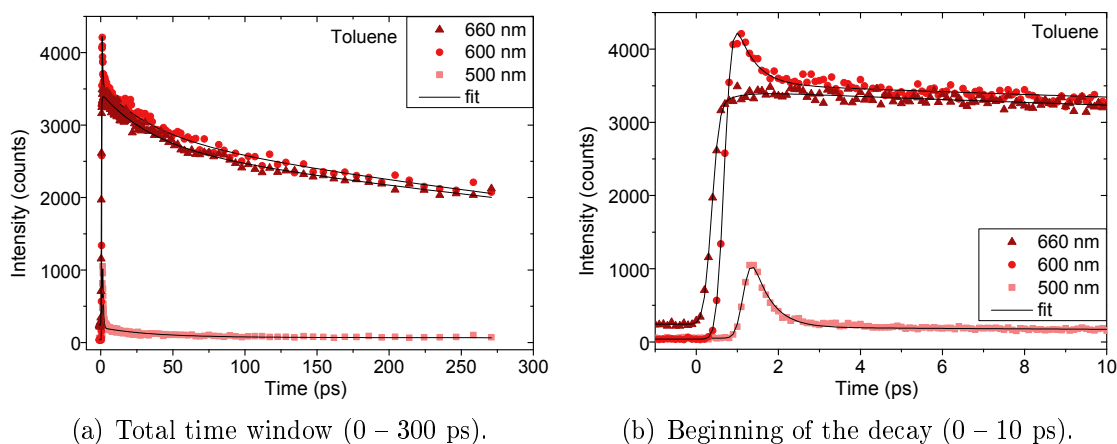


Figure 4.3. Fluorescence emission decay curves from the up-conversion measurement for 4-morpholino-HBQ in toluene.

The results of the fits, the time constants and corresponding pre-exponential factors, are presented in Table 4.4 for sample series 1 in acetonitrile, tetrahydrofuran

and toluene. The pre-exponential factors for each fitting function are shown under the corresponding fluorescence lifetimes.

Table 4.4. Fluorescence lifetimes and pre-exponential factors obtained from the fits of the up-conversion measurements in acetonitrile, tetrahydrofuran and toluene for sample series 1: 4-morpholino-HBQ, 4-methyl-HBQ, and 7-nitro-HBQ.

Compound	MeCN			THF			Toluene		
4-morpholino-HBQ	0.36 ps	26.9 ps	757 ps	0.39 ps	9.47 ps	510 ps	0.45 ps	35.4 ps	788 ps
500 nm	573	57.1	20.4	180	21.2	10.8	1470	130	21
600 nm	832	1317	2476	307	-131	1522	1530	650	2840
660 nm	-225	1415	2202	-151	12.1	1550	-218	710	2480
4-methyl-HBQ	0.31 ps	15.3 ps	627 ps	0.30 ps	9.97 ps	461 ps	0.45 ps	14.6 ps	623 ps
500 nm	599	48.6	45.9	204	17.7	-13.5	626	24	8.08
600 nm	1713	1385	2882	736	-165	1772	1204	224	794
660 nm	52.4	1676	2762	11.6	-38.9	1908	-60	520	2689
7-nitro-HBQ	0.33 ps	13.7 ps	81.9 ps	0.49 ps	34.9 ps	560 ps	0.35 ps	5.21 ps	716 ps
500 nm	2273	239	170	1299	178	41.1	744	125	72
600 nm	-114	699	1509	-371	451	1807	-644	-188	2720
660 nm	-566	986	1854	-753	699	2304	-800	0.65	1528

Emission at the shortest monitoring wavelength, 500 nm, is associated with the fluorescence of the enol tautomer. As can be observed in Table 4.4, the fastest decay component dominates the fluorescence emission at this wavelength: the pre-exponential factors for the shortest decay component are larger than the ones for the longer-living decay components. The same behaviour is visible in Figure 4.3 as well: at 500 nm, the relaxation is very fast, and there is no contribution from the longer-living decay components. Therefore, the shortest fluorescence lifetime is attributed to the relaxation of the enol excited state. If the ESIPT process is much faster than all other relaxation mechanisms from the locally excited state, the shortest lifetime describes the rate of the ESIPT reaction.

The longest-living component, on the other hand, is related to the relaxation of the keto excited state. This decay component is dominant at the longer wavelengths, which can be concluded from the greater pre-exponential factors in Table 4.4, as well as in the shape of the decay curves in Figure 4.3.

The middle component is associated with the solvent relaxation discussed in Section 2.3.5. A similar effect by the solvent-induced vibrational relaxation has been previously reported for the non-substituted HBQ in cyclohexane, with a somewhat similar time constant (ca. 8 ps [9]).

In the fitting, the instrument response function was simulated with a Gaussian function, and in all cases the width of the instrument response was below 0.20 ps. Thus, even the fastest decay component is resolvable for all compounds. Because of the short fluorescence lifetime for the locally excited state, the ESIPT reaction seems to be nearly barrierless. Furthermore, the solvent polarity has no significant effect on the shortest fluorescence lifetime for any of the compounds. The fast ESIPT process with no effect of the solvent on the rate constant suggests a negligible solvent

interference with the intramolecular hydrogen bond. [9]

The situation is somewhat different when considering the longest fluorescence lifetimes. For 4-morpholino-HBQ and 4-methyl-HBQ, there is no significant effect from the solvent. The keto excited state is quite long-living even in polar solvents, which further strengthens the assumption of the strong and solvent-independent intramolecular hydrogen bond. The lifetime of 7-nitro-HBQ, however, is reduced from the 716 ps in toluene to 560 ps in THF and to as short as 82 ps in MeCN. The same effect is observed as already was noticed in the steady-state measurements: the relaxation rate of the keto tautomer is increased in the more polar solvents, which suggests enhanced solvent interference with the intramolecular hydrogen bond for this compound.

With the total time window of the up-conversion measurements being less than 300 ps, the evaluated time constants for the longest-living decay components are somewhat inaccurate. Therefore, fluorescence lifetime measurements in a longer time scale were carried out with the TCSPC method. Figure 4.4 presents the fluorescence emission decay curves from the TCSPC measurements for the samples. The coloured curves depict the measured data points and the black solid lines the fitting function, respectively. As shown in the figure, relaxation of the keto excited state is essentially monoexponential. There is a very weak second component contributing at longer times, but its intensity is very weak. The fluorescence lifetimes for the samples are given in Table 4.5, together with the relative amplitudes of each decay component.

Table 4.5. Fluorescence lifetimes and the relative pre-exponential factors obtained from the fits of the TCSPC measurements in acetonitrile, tetrahydrofuran and toluene for sample series 1: 4-morpholino-HBQ, 4-methyl-HBQ, and 7-nitro-HBQ.

Compound	MeCN		THF		Toluene	
4-morpholino-HBQ	863 ps 0.99	4.08 ns 0.01	876 ps 0.996	5.48 ns 0.004	818 ps 0.9996	7.75 ns 0.0004
4-methyl-HBQ	650 ps 0.99	4.72 ns 0.01	654 ps 0.995	5.25 ns 0.005	690 ps 0.997	3.94 ns 0.003
7-nitro-HBQ	95.5 ps 0.998	2.28 ns 0.002	993 ps 0.98	2.6 ns 0.02	1,491 ps 0.89	2.17 ns 0.11

In Table 4.5, the main fluorescence lifetimes are shown in bold. The relative amplitudes of the decay components reveal that the longer-living component (from 2 to 7 ns) indeed is very weak. The second component is probably caused by some fluorescent impurities in the samples, and it is thus ignored.

The lifetimes obtained with the TCSPC method are in agreement with the longest-living decay components from the up-conversion measurements. The fluorescence lifetimes obtained with the up-conversion method are somewhat shorter than the ones obtained with TCSPC. Most probably, the difference is caused by the

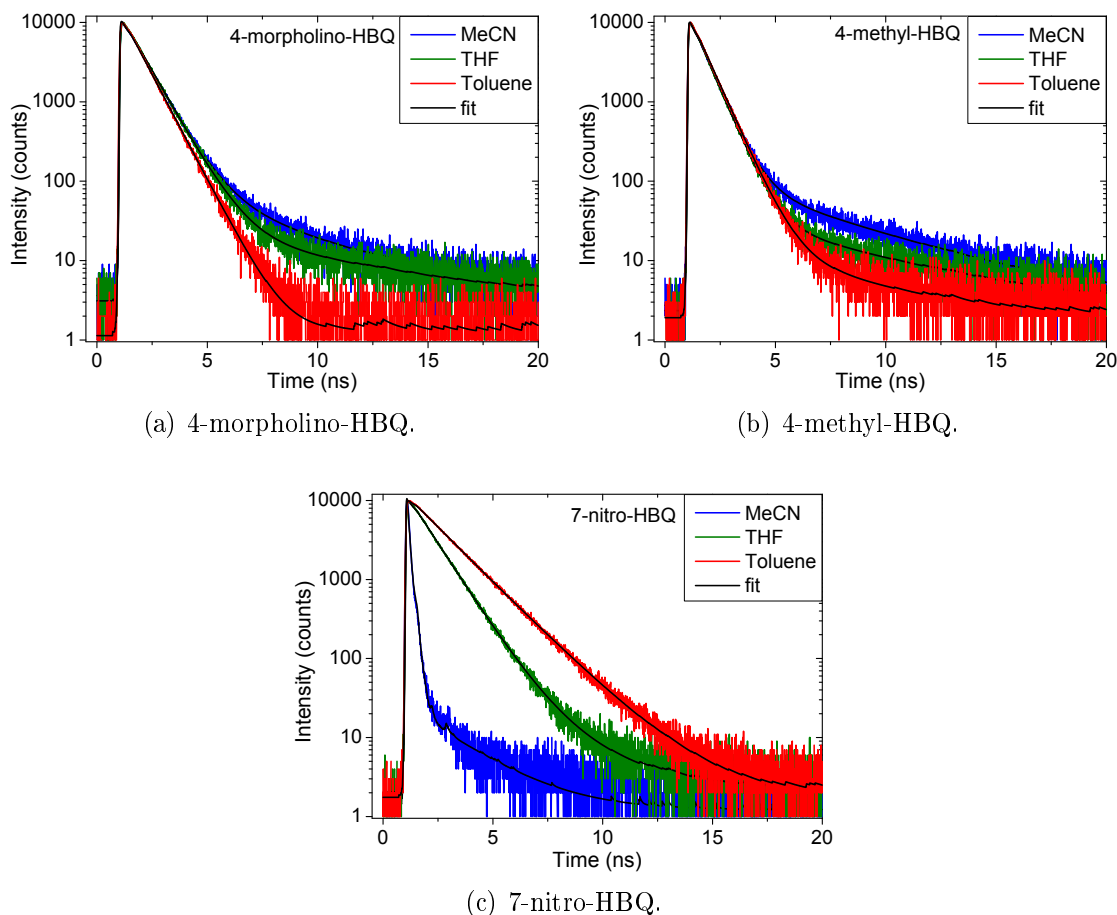


Figure 4.4. Fluorescence emission decay curves from the TCSPC measurements in acetonitrile, tetrahydrofuran and toluene for sample series 1: (a) 4-morpholino-HBQ, (b) 4-methyl-HBQ, and (c) 7-nitro-HBQ.

inaccuracy of the lifetimes obtained with up-conversion when the lifetime is much longer than the measured time window itself.

Nonetheless, similar behaviour towards solvent polarity is observed in both TCSPC and up-conversion measurements: the lifetimes of 4-morpholino-HBQ and 4-methyl-HBQ do not change with the solvent polarity. Therefore, it can be concluded that the solvent polarity does not affect the relaxation kinetics of the keto tautomer, which reinforces the idea of the strong intramolecular hydrogen bond in these two compounds.

On the contrary, for 7-nitro-HBQ, the lifetime associated with the relaxation of the keto tautomer excited state depends strongly on the solvent polarity in TCSPC measurements as well. The fluorescence lifetime is reduced from 1491 ps in toluene to 993 ps in THF and to 95.5 ps in acetonitrile. Thus, comparing THF to toluene, there is a 1.5-fold increase in the relaxation rate of the keto tautomer excited state. In MeCN, the relaxation rate is almost 16 times higher than in toluene. The changes in the relaxation rate obtained with time-resolved measurements are in good agreement

with the corresponding steady-state results. The increase in the reaction rate is associated with the weaker intramolecular hydrogen bond and the enhanced solvent perturbation on it in the nitro-substituted compounds.

4.2.2 4-cyano-HBQ, 4-tosyl-HBQ, and DHB[*a,c*]P

Fluorescence lifetimes for sample series 2 from the up-conversion measurement are presented in Table 4.6. The original data with the fitting functions are presented in Appendices 6 – 8. In the Appendix figures, each decay curve is shown in two time scales: the total time window (from 0 to ca. 100 ps), and from 0 to 10 ps.

Table 4.6. Fluorescence lifetimes and pre-exponential factors obtained from the fits of the up-conversion measurements in acetonitrile, tetrahydrofuran and toluene for sample series 2: 4-cyano-HBQ, 4-tosyl-HBQ, and DHB[*a,c*]P.

Compound	MeCN			THF			Toluene		
	τ ₁	τ ₂	τ ₃	τ ₁	τ ₂	τ ₃	τ ₁	τ ₂	τ ₃
4-cyano-HBQ	0.21 ps	1.93 ps	32.0 ps	0.13 ps	1.79 ps	35.3 ps	0.24 ps	3.27 ps	44.9 ps
610 nm	3336	412	196	2795	102	55.7	2804	348	99
710 nm	4337	1492	2792	4895	1951	1518	4901	2708	2342
750 nm	2358	990	4316	3093	641	2601	3060	1344	7527
4-tosyl-HBQ	0.14 ps	1.25 ps	36.0 ps	0.12 ps	1.41 ps	46.8 ps	0.19 ps	13.8 ps	55.7 ps
610 nm	4723	681	194	2032	181	26.4	3782	411	-239
710 nm	5247	2106	3567	2694	938	1980	9170	3717	9927
750 nm	3008	1091	5220	1021	255	3058	4821	2749	8286
DHB[<i>a,c</i>]P	0.077 ps	0.81 ps	10.7 ps	0.16 ps	8.36 ps	89.0 ps	0.080 ps	1.07 ps	14.3 ps
610 nm	3346	276	66.6	482	16.8	-6.23	3823	236	37.1
710 nm	3651	1247	1493	842	482	45.6	2250	972	1048
750 nm	2187	435	1340	429	542	351	1511	1806	3897

Similarly to the first sample series, the shortest fluorescence lifetime can be attributed to the relaxation of the enol excited state, and it is barely resolvable from the instrument response function (pulse width ca. 0.15 – 0.2 ps). Therefore, the lifetime estimations are not very reliable, and the main conclusion for 4-cyano-HBQ, 4-tosyl-HBQ, and DHB[*a,c*]P is that the fluorescence lifetime of the enol excited state is shorter than the pulse width, 0.2 ps, corresponding to an ultrafast and nearly barrierless ESIP. The second decay component is associated with the solvent relaxation, similarly to the first sample series.

The longest-living decay component corresponding to the keto tautomer relaxation is remarkably shorter for the compounds in this sample series than in sample series 1. However, the solvent polarity seems not to affect the relaxation rate of the keto excited state, similarly to sample series 1. Therefore, it can be concluded that the intramolecular hydrogen bond indeed is very strong and that interaction between the solvent and the intramolecular hydrogen bond is minimal.

Since the longest-living decay component is shorter than the total time window of the measurements in each case, the TCSPC measurements were not expected to give further information on the fluorescence lifetimes. The measured results meet the expectations quite well; the sample signals were hardly resolvable from the

instrument response function. Table 4.7 shows the fluorescence lifetimes from the TCSPC measurements for these samples, and the decay curves together with the fitting functions are presented in Appendix 9.

Table 4.7. Fluorescence lifetimes and the relative pre-exponential factors obtained from the fits of the TCSPC measurements in acetonitrile, tetrahydrofuran and toluene for sample series 2: 4-cyano-HBQ, 4-tosyl-HBQ, and DHB[*a,c*]P.

Compound	MeCN		THF		Toluene	
4-cyano-HBQ	54.86 ps 0.997	8.49 ns 0.003	55.84 ps 0.999	6.56 ns 0.001	63.49 ps 0.999	3.54 ns 0.001
4-tosyl-HBQ	63.04 ps 0.9997	1.69 ns 0.0003	65.19 ps 0.999	1.18 ns 0.001	74.19 ps 0.999	1.12 ns 0.001
DHB[<i>a,c</i>]P	35.09 ps 0.9996	1.8 ns 0.0004	36.11 ps 0.992	0.86 ns 0.008	39.33 ps 0.993	2.33 ns 0.007

Based on Table 4.7, the fluorescence emission decay for this sample series seems essentially monoexponential, with a very weak second component probably due to impurities, similarly to sample series 1. However, the lifetimes for this sample series are not reliable because the lifetimes are not much longer than the excitation pulse. Thus, any conclusions about the relaxation of the keto tautomer excited state for these compounds should be drawn based on the up-conversion measurements, and not the TCSPC measurements.

The faster relaxation of the keto tautomer in 4-methyl-HBQ and 4-tosyl-HBQ compared to 4-morpholino-HBQ and 4-methyl-HBQ can be explained by the weaker basicity of the pyridyl nitrogen in the compounds. The electron-withdrawing substituent at position 4 is located at the methylenepyridine part of the molecule, which induces a lack of electrons on the pyridyl nitrogen. This lowers the proton-binding ability of the pyridyl nitrogen (see Section 2.3.4). On the other hand, substituting an electron-donating group such as morpholine or methyl at the same position increases the electron density at the nitrogen atom, which then helps to accept the proton and stabilize the keto tautomer.

For DHB[*a,c*]P, the reason for the short relaxation lifetime is not as straightforward as for the 4-substituted compounds. Perhaps the two pyridyl-type nitrogens hamper each other's proton binding efficiency.

5 CONCLUSIONS

In this Thesis, the substituent effect on the excited-state intramolecular proton transfer (ESIPT) was studied in 10-hydroxybenzo[*h*]quinoline (HBQ) derivatives. The main focus was in comparing the spectroscopic properties in a series of compounds with different substitution at the same position. Chou *et al.* [11] have proposed a hypothesis on the substituent effect in HBQ derivatives. However, the hypothesis has been previously tested for substitution at the oxygen containing part of the molecule only. This Thesis provides the first experimental test of the hypothesis for substitution at the nitrogen containing part of the molecule.

The experimental methods used in this Thesis include steady-state absorption and emission spectroscopy, as well as time-resolved fluorescence emission spectroscopy in sub-nanosecond and sub-picosecond time scales. The measurements were carried out in three different solvents in order to investigate the effect of solvent polarity on the ESIPT process.

Apart from the compound containing an extremely electron-withdrawing group, 4-(CF₃)styryl-HBQ, ESIPT was observed in all studied compounds. The compounds behaved as expected in the hypothesis: electron-donating substituents at the methylene-pyridine part of the HBQ core shifted the keto tautomer fluorescence emission to shorter wavelengths compared to the non-substituted HBQ, which corresponds to an increase in the HOMO–LUMO energy gap. Correspondingly, electron-withdrawing substituents at the same position were noticed to shift the emission to longer wavelengths due to a decrease in the HOMO–LUMO gap.

The intramolecular hydrogen bond between the proton-donating hydroxyl group and the proton-accepting pyridyl nitrogen has been reported to be exceptionally strong in the non-substituted HBQ, because the restricted geometry of the compound forces the proton donor and acceptor to optimum position and distance relative to each other. Therefore, minor solvent polarity effect was expected in the studied HBQ derivatives as well. The results met this expectation: all compounds substituted at the methylenepyridine part of the molecule (apart from 4-(CF₃)styryl-HBQ) showed practically no solvent effect, neither in the positions of the absorption and emission maxima nor in the fluorescence quantum yields.

Only two compounds, substituted with a nitro group closer to the cyclohexa-2,4-dienone moiety, showed a remarkable solvent effect. A 1.5-fold increase in the

relaxation rate of the keto tautomer excited state was observed in 7-nitro-HBQ comparing the moderately polar tetrahydrofuran solution to the non-polar toluene. With the polar acetonitrile, the solvent effect is even greater: the relaxation rate was 16 times higher in acetonitrile than in toluene. For the other studied compounds, the fluorescence lifetime associated with the relaxation of the keto tautomer was not affected by solvent polarity.

In addition to the keto tautomer fluorescence, information on the relaxation rate of the enol tautomer was obtained with the time-resolved measurement techniques. Fluorescence lifetime related to enol tautomer relaxation was associated with the ESIPT process. Thus, the ESIPT was observed to be very fast, the lifetime being ca. 0.2 – 0.3 ps for all measured compounds. The lifetime associated with ESIPT was observed not to be affected by solvent polarity in any of the studied compounds.

With all the obtained information, it can be concluded that the intramolecular hydrogen bond indeed is very strong in most of the studied HBQ derivatives, and thus a remarkable solvent polarity effect was not observed, neither on the rate of the ESIPT process, nor in the relaxation of the proton transfer tautomer (keto tautomer). Differences in the keto tautomer relaxation rate arise from the different substitutions of the HBQ core. With electron-withdrawing substituents at the methylenepyridine part of the molecule, the keto tautomer relaxation was observed to be much faster than with electron-donating substituents at the same position. The difference is explained by the different proton-binding ability of the pyridyl nitrogen in the different compounds.

BIBLIOGRAPHY

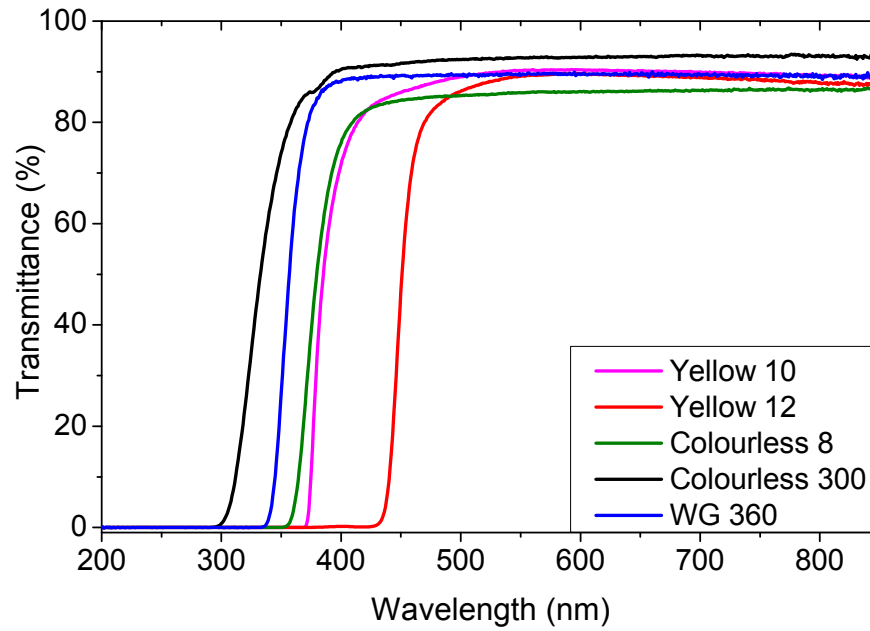
- [1] E. Caldin and V. Gold. *Proton-transfer reactions*. Chapman and Hall, London, 1975. 448 p.
- [2] A. Douhal, F. Lahmani, and A.H. Zewail. Proton-transfer reaction dynamics. *Chemical Physics*, 207(2-3):477–498, 1996.
- [3] S.S. Zumdahl. *Chemical Principles*. Houghton Mifflin Company, Boston, 5th edition, 2005. 1070 p.
- [4] A.B. Kotlyar, N. Borovok, S. Kiryati, E. Nachliel, and M. Gutman. The Dynamics of Proton Transfer at the C Side of the Mitochondrial Membrane: Picosecond and Microsecond Measurements. *Biochemistry*, 33(4):873–879, 1994.
- [5] A.P. Demchenko, editor. *Advanced Fluorescence Reporters in Chemistry and Biology I: Fundamentals and Molecular Design*, volume 8 of *Springer Series on Fluorescence*. Springer-Verlag, Berlin Heidelberg, 2010. 389 p.
- [6] A. Sytnik and J.C. Del Valle. Steady-State and Time-Resolved Study of the Proton-Transfer Fluorescence of 4-Hydroxy-5-azaphenanthrene in Model Solvents and in Complexes with Human Serum Albumin. *Journal of physical chemistry*, 99(34):13028–13032, 1995.
- [7] A. Sytnik and M. Kasha. Excited-state intramolecular proton transfer as a fluorescence probe for protein binding-site static polarity. *Proceedings of the National Academy of Sciences of the United States of America*, 91(18):8627–8630, 1994.
- [8] P.-T. Chou and M.L. Martinez. Photooxygenation of 3-hydroxyflavone and molecular design of the radiation-hard scintillator based on the excited-state proton transfer. *Radiation Physics and Chemistry*, 41(1-2):373–378, 2 1993.
- [9] P.-T. Chou, Y.-C. Chen, W.-S. Yu, Y.-H. Chou, C.-Y. Wei, and Y.-M. Cheng. Excited-state Intramolecular Proton Transfer in 10-Hydroxybenzo[h]quinoline. *Journal of Physical Chemistry A*, 105(10):1731–1740, 2001.
- [10] A.U. Khan and M. Kasha. Mechanism of four-level laser action in solution excimer and excited-state proton-transfer cases. *Proceedings of the National Academy of Sciences*, 80(6):1767, 1983.
- [11] K.-Y. Chen, C.-C. Hsieh, Y.-M. Cheng, C.-H. Lai, and P.-T. Chou. Extensive spectral tuning of the proton transfer emission from 550 to 675 nm *via* a rational derivatization of 10-hydroxybenzo[h]quinoline. *Chemical Communications*, (42):4395–4397, 2006.

- [12] P.-T. Chou and C.-Y. Wei. Photophysics of 10-Hydroxybenzo[*h*]quinoline in Aqueous Solution. *Journal of Physical Chemistry*, 100(42):17059–17066, 1996.
- [13] T. Engel and P. Reid. *Physical Chemistry*. Benjamin Cummings, San Francisco, 2006. 1061 p.
- [14] B. Valeur. *Molecular Fluorescence: Principles and Applications*. Wiley-VHC Verlag GmbH, Weinheim, 2001. 381 p.
- [15] N.V. Tkachenko. *Optical Spectroscopy: Methods and Instrumentations*. Elsevier Science & Technology, Amsterdam, 2006. 307 p.
- [16] P.A. Tipler and R.A. Llewellyn. *Modern Physics*. W.H. Freeman, New York, 4th edition, 2003. 731 p.
- [17] J.R. Lakowicz. *Principles of Fluorescence Spectroscopy*. Springer Science + Business Media, New York, 3rd edition, 2006. 954 p.
- [18] P.W. Atkins and R. Friedman. *Molecular Quantum Mechanics*. Oxford University Press, Oxford, 5th edition, 2011. 592 p.
- [19] A.D. McNaught and A. Wilkinson, editors. *Compendium of Chemical Terminology (Gold Book)*. International Union of Pure and Applied Chemistry, 2011. XML on-line version: <http://goldbook.iupac.org> (2006-) created by M. Nic, J. Jirat, B. Kosata; updates compiled by A. Jenkins.
- [20] G.G. Stokes. On the Change of Refrangibility of Light. *Philosophical Transactions of the Royal Society of London*, 142:463–562, 1852.
- [21] P.S. Nobel. *Physicochemical and Environmental Plant Physiology*. Academic Press, Oxford, 4th edition, 2009. 582 p.
- [22] C.-C. Hsieh, C.-M. Jiang, and P.-T. Chou. Recent Experimental Advances on Excited-State Intramolecular Proton Coupled Electron Transfer Reaction. *Accounts of Chemical Research*, 43(10):1364–1374, 2010.
- [23] C.-C. Hsieh, Y.-M. Cheng, C.-J. Hsu, K.-Y. Chen, and P.-T. Chou. Spectroscopy and Femtosecond Dynamics of Excited-State Proton Transfer Induced Charge Transfer Reaction. *The Journal of Physical Chemistry A*, 112(36):8323–8332, 2008.

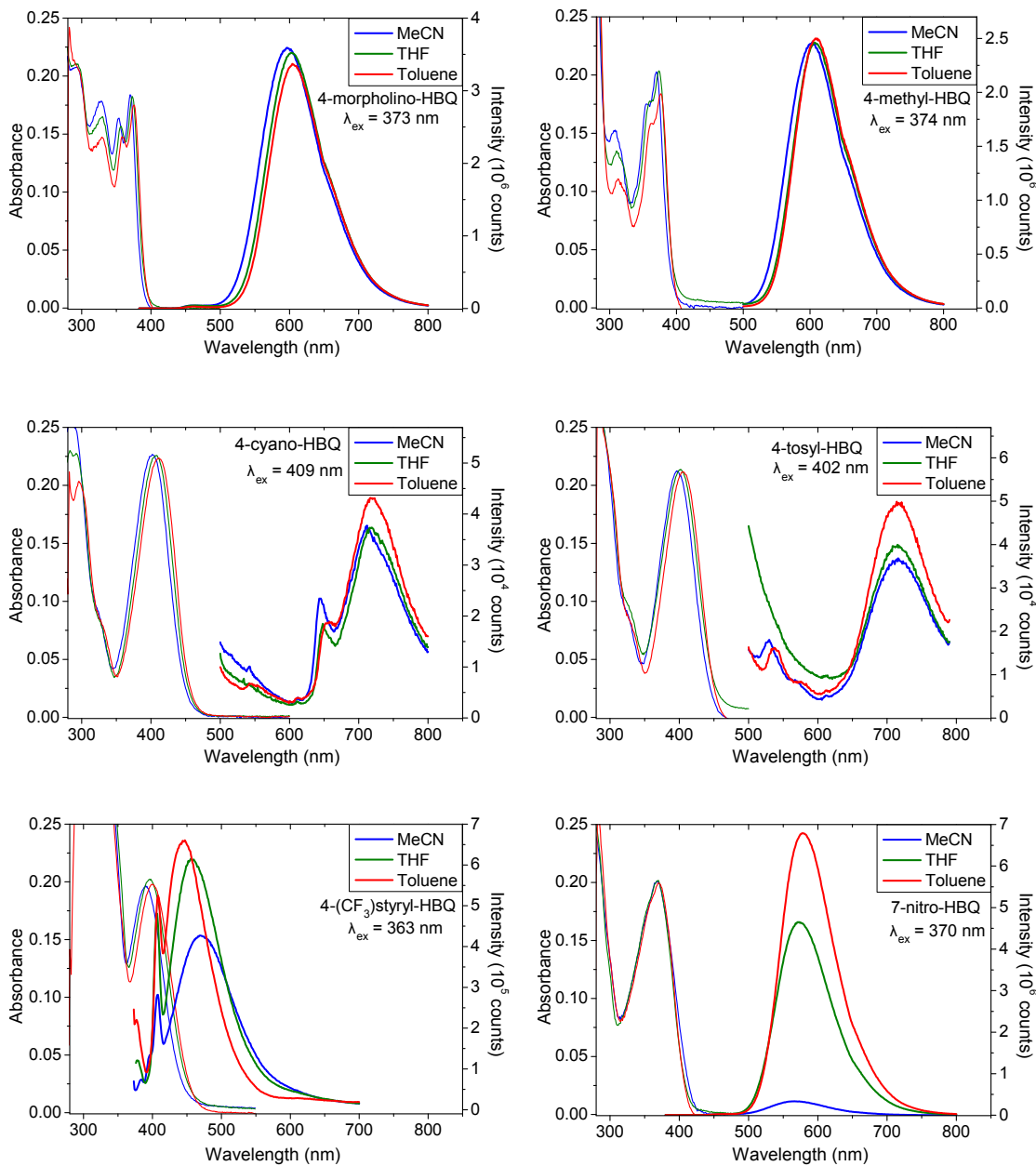
- [24] P.-T. Chou, S.-C. Pu, Y.-M. Cheng, W.-S. Yu, Y.-C. Yu, F.-T. Hung, and W.-P. Hu. Femtosecond Dynamics on Excited-State Proton/ Charge-Transfer Reaction in 4'-*N,N*-Diethylamino-3-hydroxyflavone. The Role of Dipolar Vectors in Constructing a Rational Mechanism. *Journal of Physical Chemistry A*, 109(17):3777–3787, 2005.
- [25] P.F. Barbara, P.K. Walsh, and L.E. Brus. Picosecond Kinetic and Vibrationally Resolved Spectroscopic Studies of Intramolecular Excited-State Hydrogen Atom Transfer. *Journal of Physical Chemistry*, 93(1):29–34, 1989.
- [26] G.C. Pimentel and A.L. McClellan. *The Hydrogen Bond*. W.H. Freeman, New York, 1960. 475 p.
- [27] O.-H. Kwon and A.H. Zewail. Double proton transfer dynamics of model DNA base pairs in the condensed phase. *Proceedings of the National Academy of Sciences of the United States of America*, 104(21):8703–8708, 2007.
- [28] M. Négrerie, F. Gai, S.M. Bellefeuille, and J.W. Petrich. Photophysics of a Novel Optical Probe: 7-Azaindole. *Journal of Physical Chemistry*, 95(22):8663–8670, 1991.
- [29] S. Takeuchi and T. Tahara. The answer to concerted versus step-wise controversy for the double proton transfer mechanism of 7-azaindole dimer in solution. *Proceedings of the National Academy of Sciences of the United States of America*, 104(13):5285–5290, 2007.
- [30] P.O. Löwdin. Quantum Genetics and the Aperiodic Solid: Some Aspects on the Biological Problems of Heredity, Mutations, Aging, and Tumors in View of the Quantum Theory of the DNA Molecule. *Advances in Quantum Chemistry*, 2:213–360, 1966.
- [31] A. Sytnik, D. Gormin, and M. Kasha. Interplay between excited-state intramolecular proton transfer and charge transfer in flavonols and their use as protein-binding-site fluorescence probes. *Proceedings of the National Academy of Sciences*, 91(25):11968–11972, 1994.
- [32] B.G. Levi. The 2008 Nobel Chemistry Prize honors the development of a fluorescent tag for bioscience. *Physics Today*, 61:20–22, 2008.
- [33] J.H. Burroughes, D.D.C. Bradley, A.R. Brown, R.N. Marks, K. Mackay, R.H. Friend, P.L. Burns, and A.B. Holmes. Light-emitting diodes based on conjugated polymers. *Nature*, 347(6293):539–541, 1990.

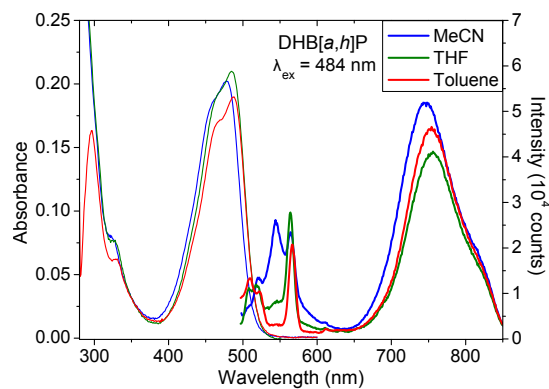
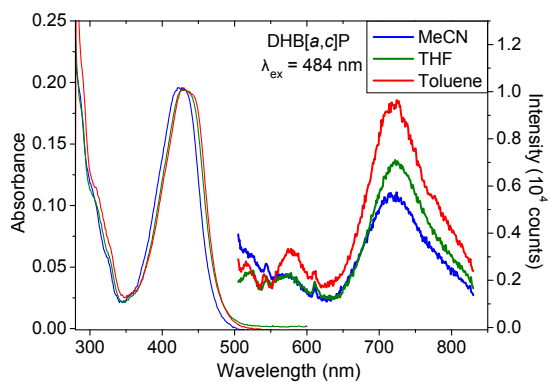
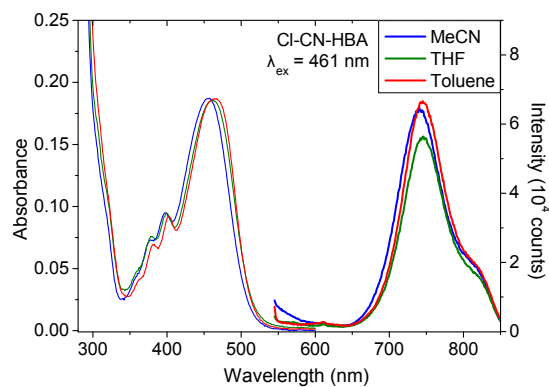
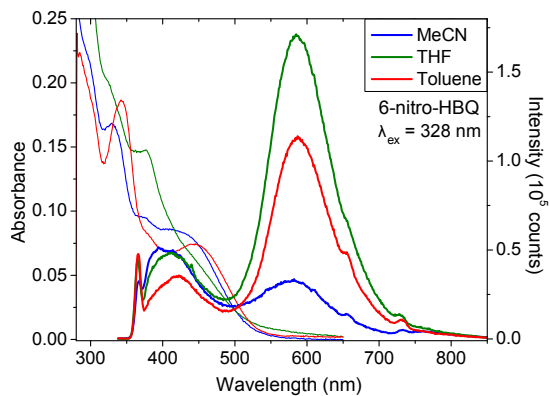
- [34] C.W. Tang and S.A. VanSlyke. Organic electroluminescent diodes. *Applied Physics Letters*, 51(12):913–915, 1987.
- [35] J.E. Kwon and S.Y. Park. Advanced Organic Optoelectronic Materials: Harnessing Excited-State Intramolecular Proton Transfer (ESIPT) Process. *Advanced Materials*, 23(32):3615–3642, 2011.
- [36] A.U. Acuña, F. Amat, J. Catalán, A. Costela, J.M. Figuera, and J.M. Muñoz. Pulsed Liquid Lasers from Proton Transfer in the Excited State. *Chemical Physics Letters*, 132(6):567–569, 1986.
- [37] P. Chou, D. McMorro, T.J. Aartsma, and M. Kasha. The Proton-Transfer Laser. Gain Spectrum and Amplification of Spontaneous Emission of 3-Hydroxyflavone. *Journal of Physical Chemistry*, 88(20):4596–4599, 1984.
- [38] K.-I. Sakai, T. Tsuzuki, Y. Itoh, M. Ichikawa, and Y. Taniguchi. Using proton-transfer laser dyes for organic laser diodes. *Applied Physics Letters*, 86(8):1–3, 2005.
- [39] J. Shah. Ultrafast Luminescence Spectroscopy Using Sum Frequency Generation. *IEEE Journal of Quantum Electronics*, 24(2):276–288, 1988.
- [40] U. Resch-Genger, editor. *Standardization and Quality Assurance in Fluorescence Measurements I: Techniques*, volume 5 of *Springer Series on Fluorescence*. Springer, Berlin Heidelberg, 2008. 700 p.
- [41] W.M. Haynes and D.R. Lide, editors. *CRC Handbook of Chemistry and Physics*. CRC Press/Taylor and Francis, Boca Raton, 92th edition, Internet Version 2011-2012.

APPENDIX 1: TRANSMITTANCE SPECTRA OF THE FILTERS

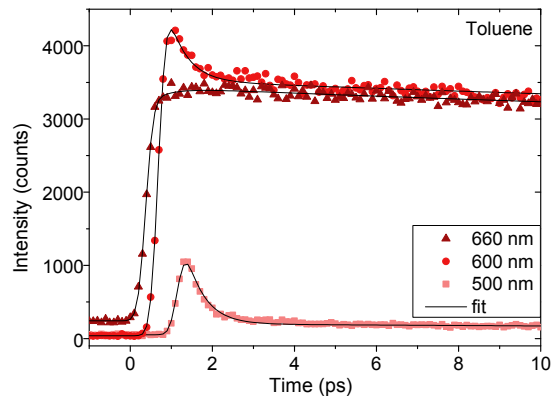
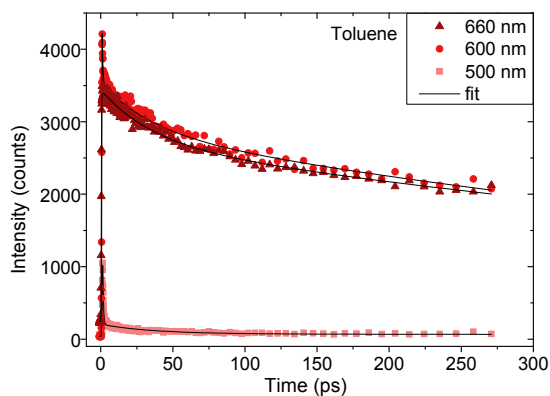
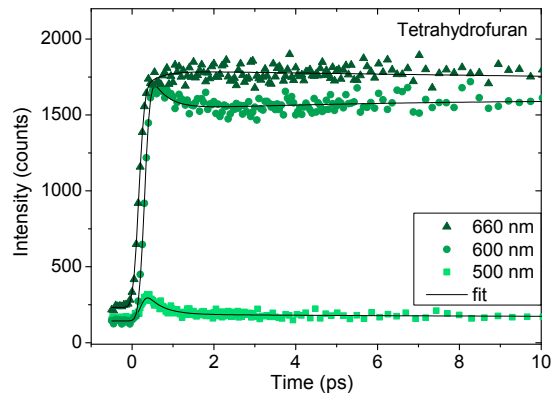
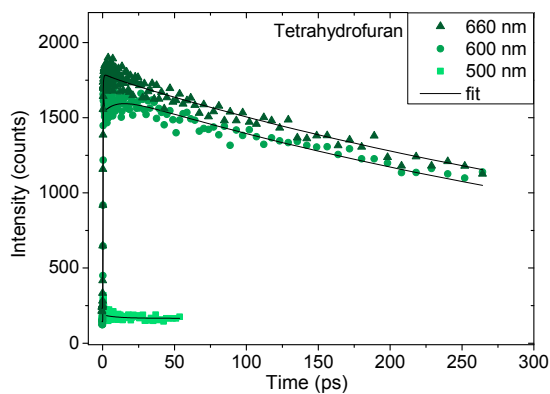
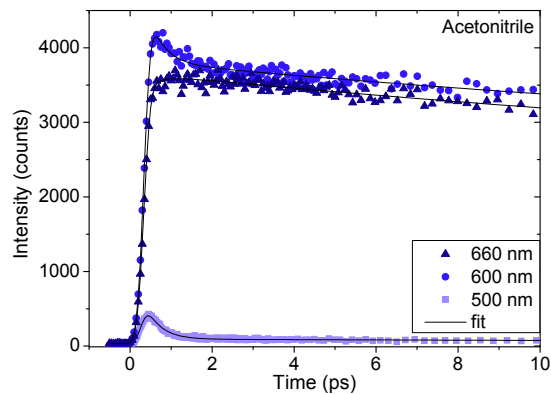
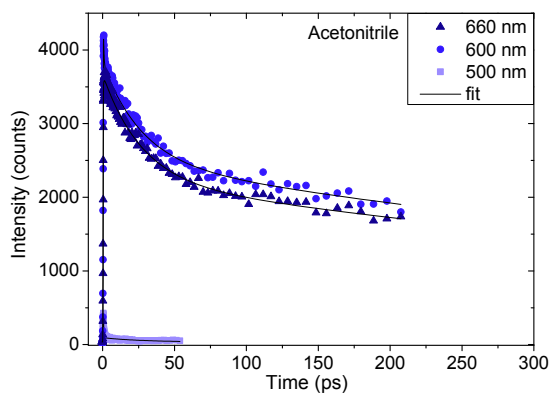


APPENDIX 2: ABSORPTION AND EMISSION SPECTRA OF THE COMPOUNDS

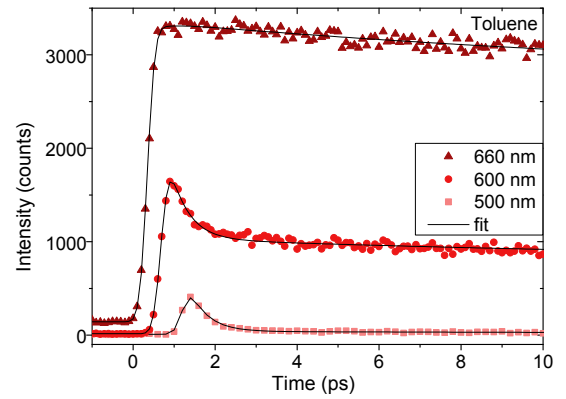
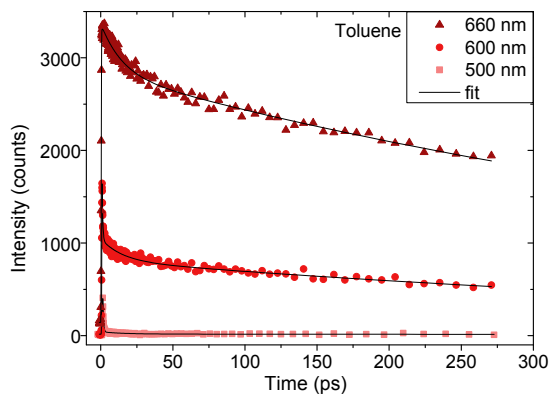
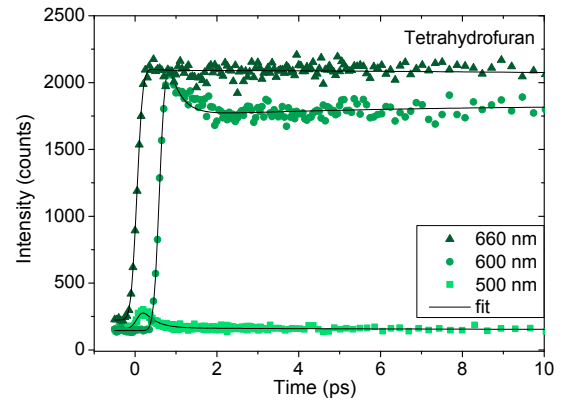
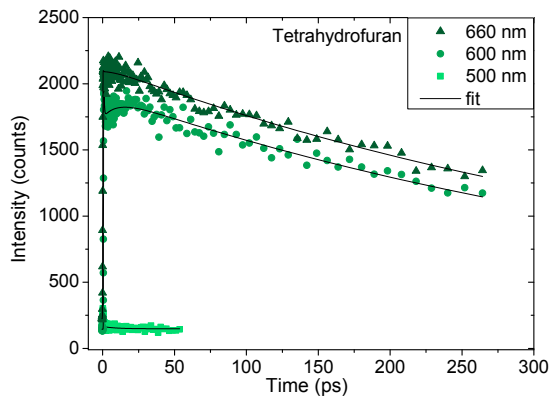
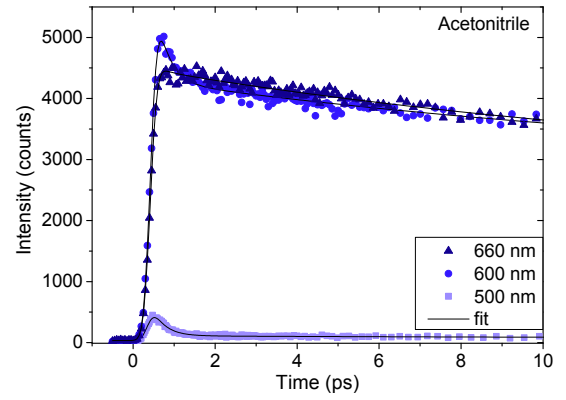
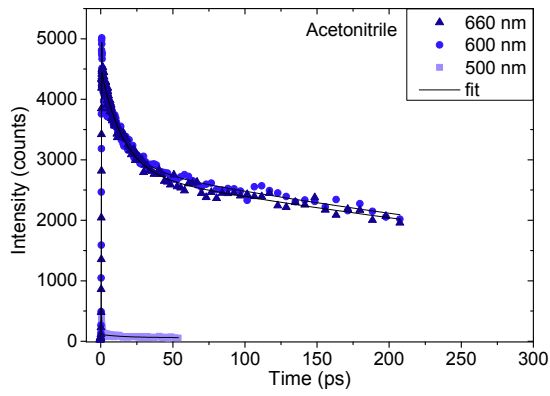




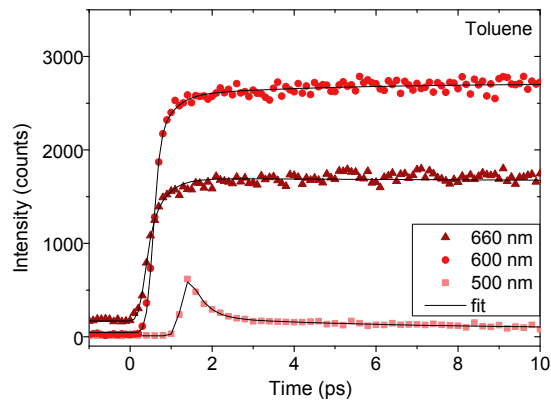
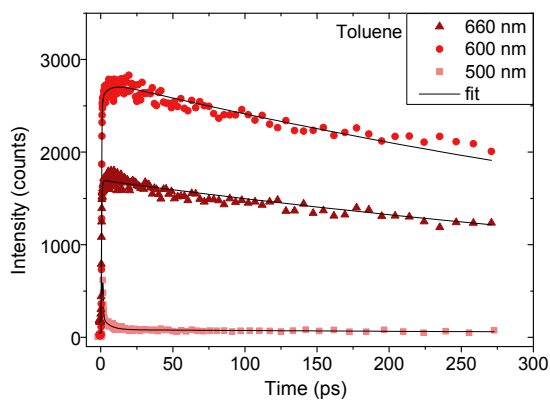
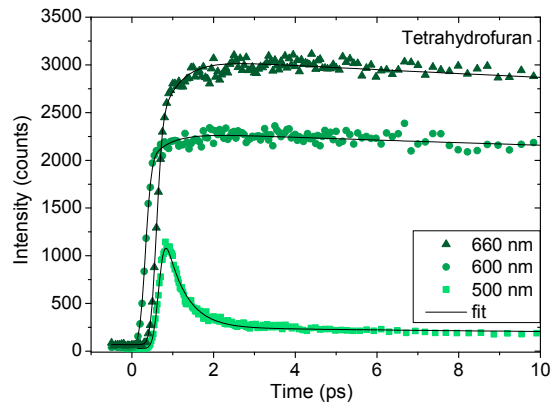
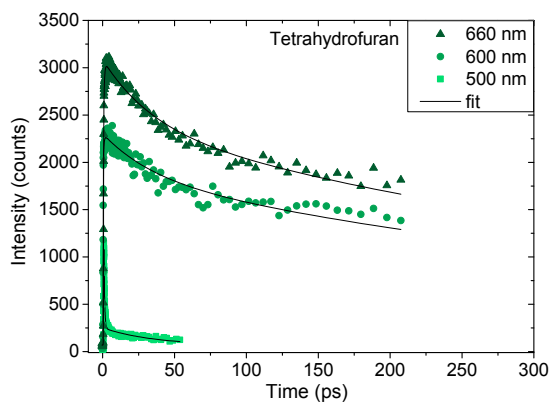
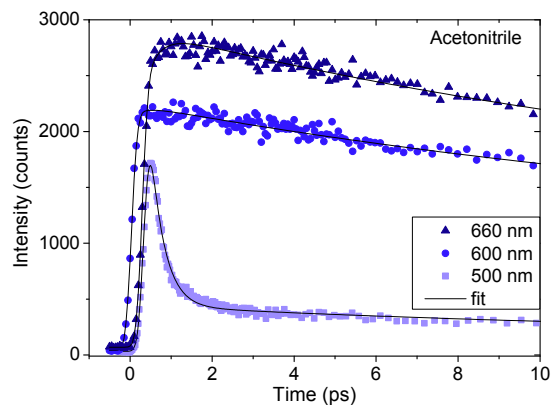
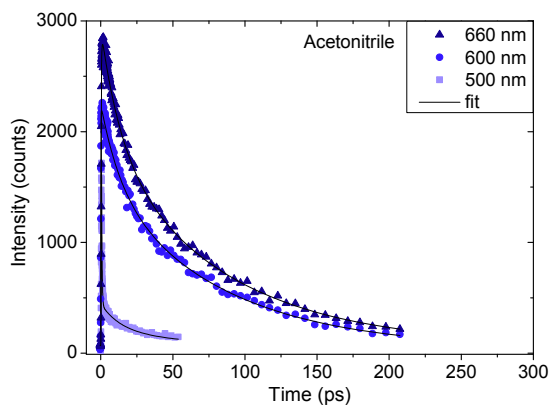
APPENDIX 3: EMISSION DECAYS FROM UP-CONVERSION FOR 4-MORPHOLINO-HBQ



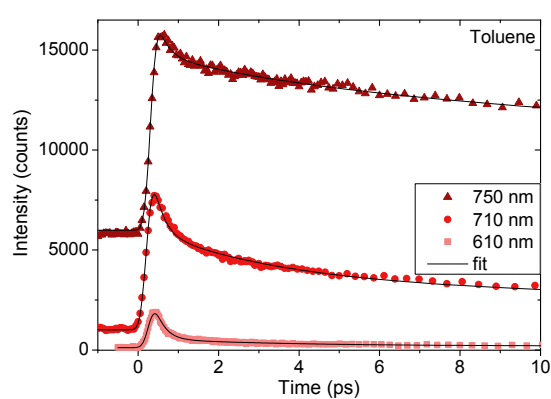
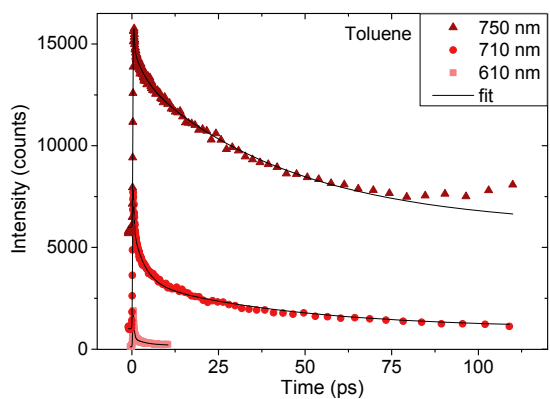
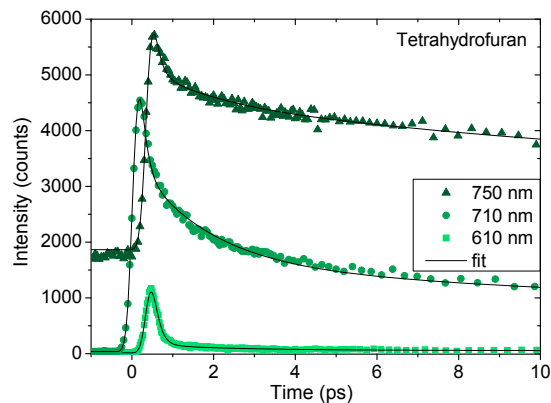
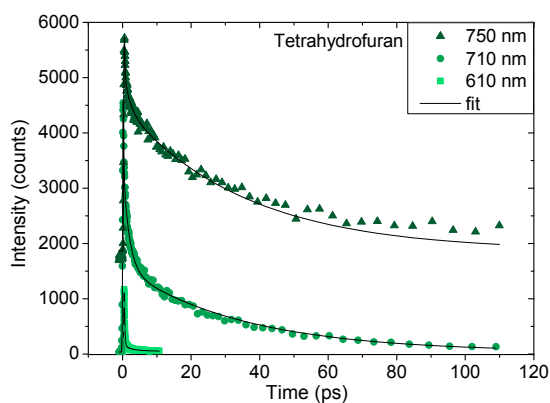
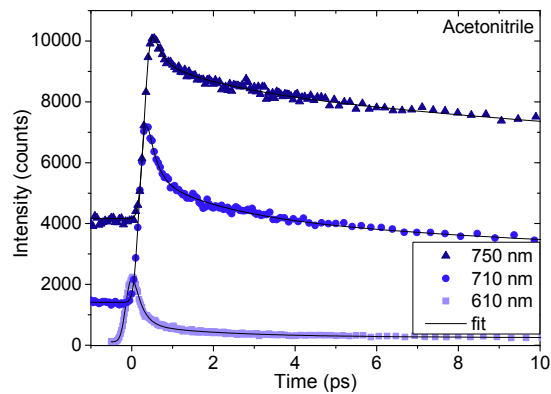
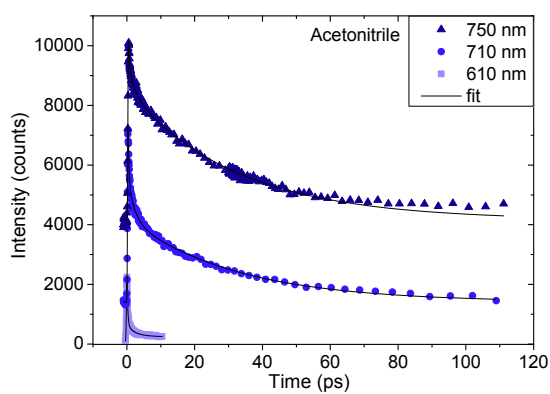
APPENDIX 4: EMISSION DECAYS FROM UP-CONVERSION FOR 4-METHYL-HBQ



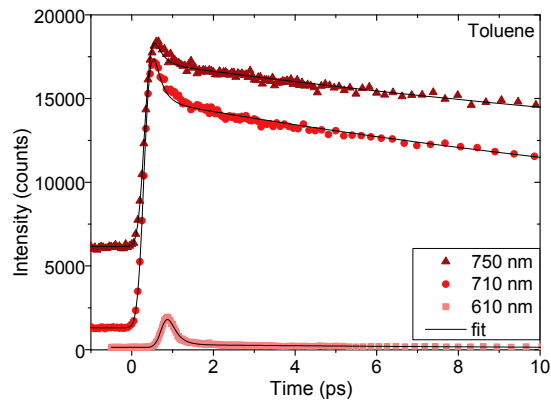
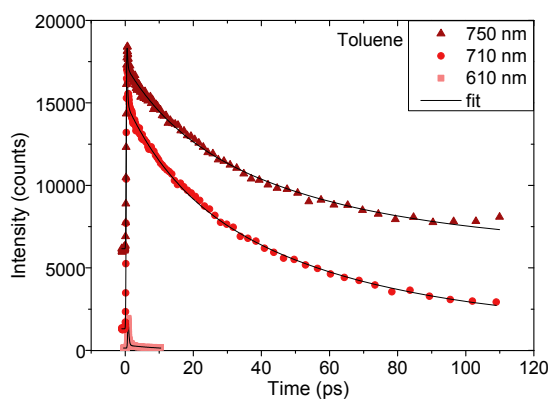
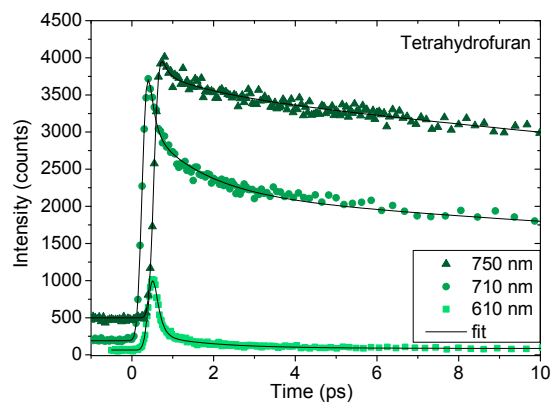
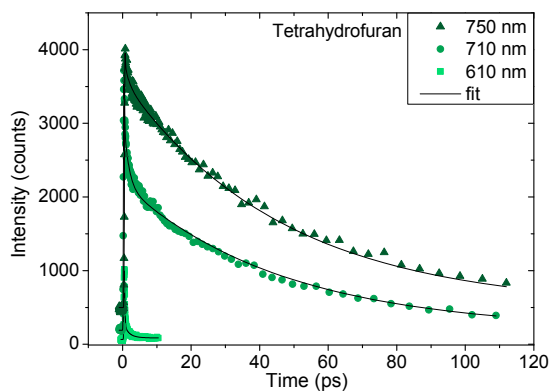
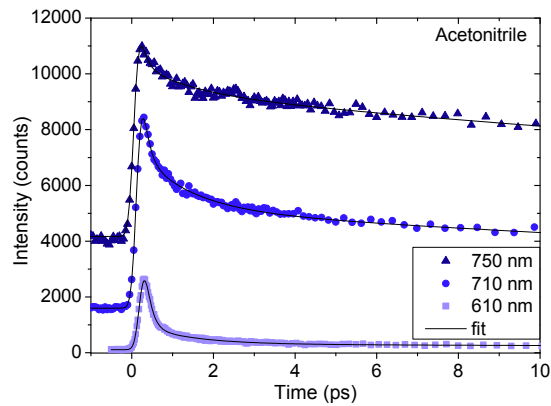
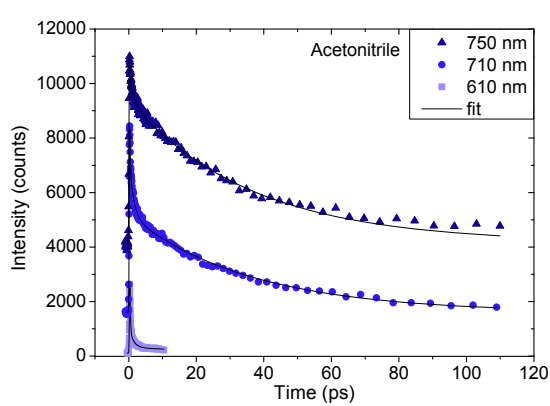
APPENDIX 5: EMISSION DECAYS FROM UP-CONVERSION FOR 7-NITRO-HBQ



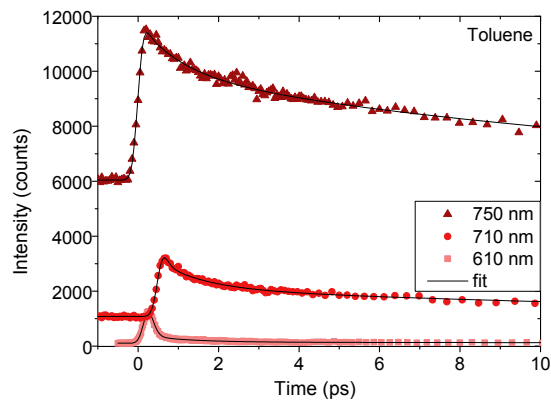
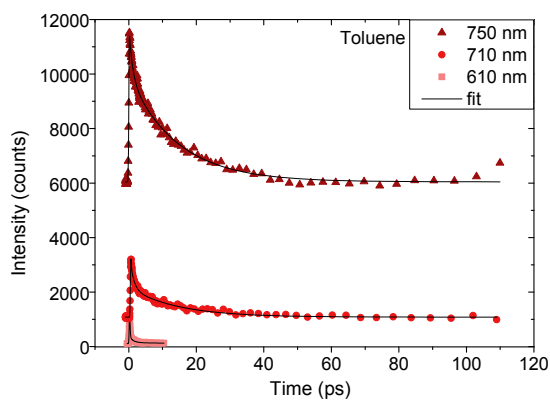
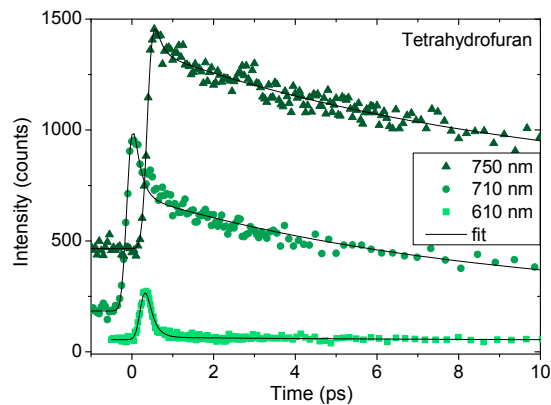
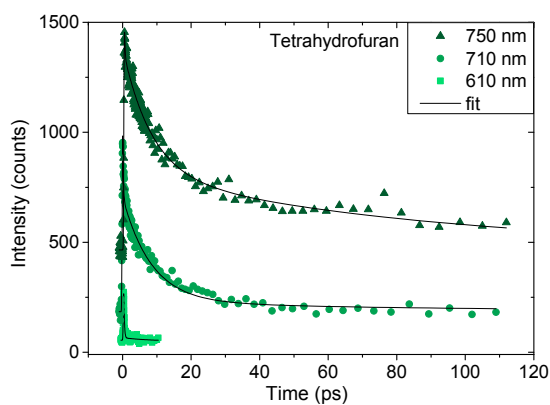
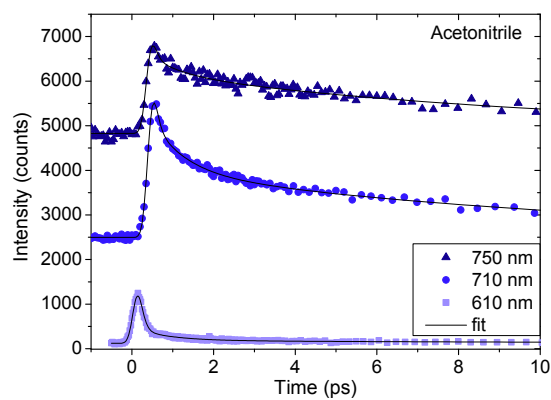
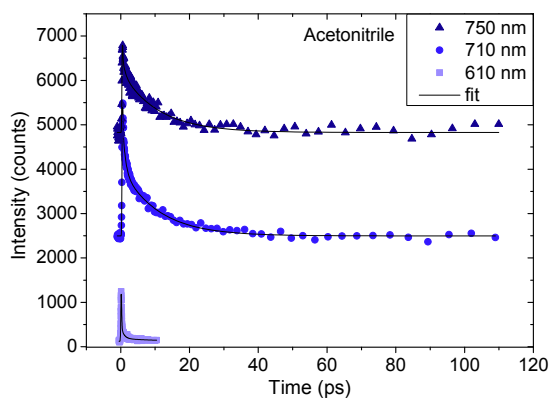
APPENDIX 6: EMISSION DECAYS FROM UP-CONVERSION FOR 4-CYANO-HBQ



APPENDIX 7: EMISSION DECAYS FROM UP-CONVERSION FOR 4-TOSYL-HBQ



APPENDIX 8: EMISSION DECAYS FROM UP-CONVERSION FOR DHB[a,c]P



APPENDIX 9: EMISSION DECAY CURVES FROM TCSPC FOR 4-CYANO-HBQ, 4-TOSYL-HBQ, AND DHB[a,c]P

